U.S. DEPARTMENT OF COMMERCE
National Technical Information Service

PB-292 108

Multiwavelength Transmissometer for Measuring Mass Concentration of Particulate Emissions

Ford Aerospace and Communications Corp, Newport Beach, CA

Prepared for

Environmental Sciences Research Lab, Research Triangle Park, NC

Feb 79

United States
Environmental Protection
Agency

Environmental Sciences Research
Laboratory
Research Triangle Park NC 27711

EPA-600/2-79-022
February 1979

Research and Development

PB 292108

EPA

Multiwavelength Transmissometer for Measuring Mass Concentration of Particulate Emissions

REPRODUCED BY
NATIONAL TECHNICAL
INFORMATION SERVICE
U. S. DEPARTMENT OF COMMERCE
SPRINGFIELD, VA. 22161

RESEARCH REPORTING SERIES

Research reports of the Office of Research and Development, U S Environmental Protection Agency, have been grouped into nine series These nine broad categories were established to facilitate further development and application of environmental technology Elimination of traditional grouping was consciously planned to foster technology transfer and a maximum interface in related fields The nine series are

1. Environmental Health Effects Research
2. Environmental Protection Technology
3. Ecological Research
4. Environmental Monitoring
5. Socioeconomic Environmental Studies
6. Scientific and Technical Assessment Reports (STAR)
7. Interagency Energy-Environment Research and Development
8. "Special" Reports
9. Miscellaneous Reports

This report has been assigned to the ENVIRONMENTAL PROTECTION TECHNOLOGY series. This series describes research performed to develop and demonstrate instrumentation, equipment, and methodology to repair or prevent environmental degradation from point and non-point sources of pollution. This work provides the new or improved technology required for the control and treatment of pollution sources to meet environmental quality standards.

This document is available to the public through the National Technical Information Service, Springfield, Virginia 22161.

TECHNICAL REPORT DATA
(Please read Instructions on the reverse before completing)

1. REPORT NO. EPA-600/2-79-022	2.
3. RECIPIENT'S ACCESSION NO. PB292108	
4. TITLE AND SUBTITLE MULTIWAVELENGTH TRANSMISSOMETER FOR MEASURING MASS CONCENTRATION OF PARTICULATE EMISSIONS	5. REPORT DATE February 1979 6. PERFORMING ORGANIZATION CODE
7. AUTHOR(S) Eli Reisman	8. PERFORMING ORGANIZATION REPORT NO.
9. PERFORMING ORGANIZATION NAME AND ADDRESS Ford Aerospace and Communications Corporation Aeronutronic Division Newport Beach, California 92663	10. PROGRAM ELEMENT NO. 1AA010 (1AD712) 11. CONTRACT/GRANT NO. 68-02-2206
12. SPONSORING AGENCY NAME AND ADDRESS Environmental Sciences Research Laboratory - RTP, NC Office of Research and Development U.S. Environmental Protection Agency Research Triangle Park, N.C. 27711	13. TYPE OF REPORT AND PERIOD COVERED Final 7/75 - 5/78 14. SPONSORING AGENCY CODE EPA/600/09
15. SUPPLEMENTARY NOTES	

16. ABSTRACT

A multiwavelength transmissometer potentially capable of making near-real-time measurements of particulate mass concentration in industrial stacks was developed. A computer program is employed to interpret the transmissometer data and translate the results into mass concentration. The transmissometer utilizes four different wavelengths and records the opacity of the particulate emissions at each wavelength. Since the response at each wavelength depends on the size of the particles, the relative values of opacity provide the computer with information on particle sizes. If the computer is also given the wavelength dependence of the optical indices of refraction and guidelines as to the most probable distribution forms, the computer can adjust the mean and spread of the distribution to find a best fit to the experimental data. It then uses this information to compute the mass concentration. The theory behind the measurement technique, a laboratory demonstration of the technique, and the optical and electrical design of the instrument are discussed.

17. KEY WORDS AND DOCUMENT ANALYSIS

a. DESCRIPTORS	b. IDENTIFIERS/OPEN ENDED TERMS	c. COSATI Field/Group
* Air pollution * Flue dust * Particles * Weight (mass) * Transmissometers * Computers		13B 21B 14B 09B

18. DISTRIBUTION STATEMENT RELEASE TO PUBLIC	19. SECURITY CLASS *(This Report)* UNCLASSIFIED 20. SECURITY CLASS *(This page)* UNCLASSIFIED	21. NO. OF PAGES 64 22. PRICE A04 - A01

EPA Form 2220-1 (Rev. 4-77) PREVIOUS EDITION IS OBSOLETE

EPA-600/2-79-022
February 1979

MULTIWAVELENGTH TRANSMISSOMETER FOR MEASURING MASS CONCENTRATION OF PARTICULATE EMISSIONS

by

E. Reisman
Ford Aerospace & Communications Corporation
Aeronutronic Division
Newport Beach, California 92663

Contract No. 68-02-2206

Project Officer

W. D. Conner
Emission Measurement and Characterization Division
Environmental Sciences Research Laboratory
Research Triangle Park, North Carolina 27711

ENVIRONMENTAL SCIENCES RESEARCH LABORATORY
OFFICE OF RESEARCH AND DEVELOPMENT
U.S. ENVIRONMENTAL PROTECTION AGENCY
RESEARCH TRIANGLE PARK, NORTH CAROLINA 27711

DISCLAIMER

This report has been reviewed by the Environmental Sciences Research Laboratory, U.S. Environmental Protection Agency, and approved for publication. Approval does not signify that the contents necessarily reflect the views and policies of the U.S. Environmental Protection Agency, nor does mention of trade names or commercial products constitute endorsement or recommendation for use.

ABSTRACT

A field-worthy multiwavelength transmissometer potentially capable of making near-real-time measurements of particulate mass concentration in industrial stacks was fabricated and delivered. A computer program is employed to interpret the transmissometer data and translate the results into mass concentration. The transmissometer utilizes four different wavelengths and records the opacity of the particulate emissions at each wavelength. Since the response at each wavelength depends on the size of the particles, the relative values of the opacity provide the computer with information on particle sizes. If the computer is also given the wavelength dependence of the optical indices of refraction and guidelines as to the most probable distribution forms, the computer can adjust the mean and spread of the distribution to find a best fit to the experimental data. It then uses this information to compute the mass concentration. The theory behind the measurement technique, and a laboratory demonstration of the technique are discussed. Also discussed are the optical and electrical design of the instrument.

CONTENTS

Abstract iii
Figures vi
Tables vii

1. Introduction 1
2. Conclusions 2
3. Recommendations 4
4. Fundamental Considerations and General Background 5
   Scattering Theory 5
   Related Problems 7
5. The Transmissometer. 15
   General Description 15
   Electrical System 27
6. Laboratory Studies 41
   Dust Chamber 41
   Particulates 43
   Analysis. 44
   Test Results 46

References. 54

Preceding page blank

FIGURES

Number		Page
1	Size distribution of cement as determined by Cascade Impacters	6
2	Experimental values of extinction coefficient, K, for 1 and 2 micron water droplets	8
3	Dependence of scattering efficiency on size parameter for water droplets.	9
4	Experimental values of K versus $1/\lambda$ fitted to Q curve	10
5	Transmitter/receiver unit	17
6	Transmitter/receiver unit (cover removed)	18
7	Retro-unit.	19
8	Retro-unit (cover removed).	20
9	Schematic illustration of two spectral channels of the Multiwavelength Transmissometer	22
10	Split-cats-eye retroreflector unit.	23
11	Schematic diagram of the transmitter/receiver unit.	25
12	Electrical interconnections	28
13	Transmitter/receiver wiring diagram	29
14	Sync pick-up schematic.	30
15	Preamplifier schematics	31
16	Electrical units.	32
17	Interior of Nernst power supply unit.	34
18	Nernst power supply schematic	35
19	Reference voltage schematic	36

FIGURES (Continued)

Number		Page
20	Sync amplifier schematic.	37
21	Sync timing sequence.	38
22	AGC amplifier schematic	39
23	Smoke stack simulator for laborator tests	42
24	Mass concentration correlation between optical measurement and sampling measurement.	47
25	Particle size distribution function	48
26	Particle size distribution function	49
27	Particle size distribution function	50
28	Mass concentration correlation between optical measurement and sampling measurement.	51

TABLES

1	Calculated absorptance by gases in the optical windows. . . .	13
2	Conjugate points for the multiwavelength transmissometer optics.	24
3	Summary of test results	52

SECTION 1

INTRODUCTION

As techniques to monitor and control pollution evolve with time, new requirements and specifications were generated that gave rise to new and improved specialized types of instrumentation. The earliest forms of regulation concerned plume opacity, since it was the most obvious indication of particulate pollution. Because opacity is by its very nature an optical phenomena, there are now a number of optical systems both manual and automatic that do an excellent monitoring job. The more physical properties of particulate emissions, such as mass concentration and size, are still primarily measured by sampling techniques. In the case of mass concentration, gravimetric analysis of the samples is generally used. In the latter case, some form of aerodynamic sizing or microscopic examination is used.

There are several optical approaches currently under development that will yield a measurement of mass concentration and size in real time (or near real time). These approaches generally rely on a prior knowledge of the optical properties of the particulates so that the observed interaction can be both measured and determined from scattering theory. Since scattering is a size dependent phenomenon, a suitable number of observations can be reduced to yield information about the size and, hence, about the mass concentration of the particles. The section that follows covers the features of scattering theory that constitute the underlying principles upon which such systems are based. One system in particular, a multiwavelength transmissometer, is described in detail in Section 3. Test performance data is presented in Section 4.

SECTION 2

CONCLUSIONS

Since the task of the program was to build and deliver a field-worthy multiwavelength transmissometer, it is difficult to reach any conclusions within the framework of the program beyond the obvious one; that the task was accomplished. If the discussion is allowed to encompass the associated independent research that has been done over a number of years, it is then possible to draw a variety of conclusions. These conclusions will be made without detailing the programs since the relevance of the conclusion to the subject is readily apparent. They are as follows:

- Each different type of industrial stack effluent studied appears to have an optical signature commensurate with aerodynamic size measurement.

- Proper interpretation of signatures requires information on the wavelength dependence of the refractive indices of the particulates. This can be obtained by techniques described in Section 4 or by obtaining presized monodispersed samples and fitting to scattering theory.

- Independent determination of the distributional form should be obtained by sampling the type of stack to be optically monitored.

- Observational wavelengths should be selected at windows in the absorption spectra of the stack gases and should encompass the size distribution. It is best not to work at wavelengths where the index is varying rapidly.

- Since an observation at a given wavelength is not completely independent of a second observation at a second wavelength, it is better to over determine and use a "least squares" fit rather than seek a precise solution. This can be done by hand through use of nomographs, or automatically with a data processor.

- A system equipped with automatic data processing can provide an accurate, continuous readout of particle size and mass concentration.

- A system built for one type of effluent can be used for another by making minor software modifications.

SECTION 3

RECOMMENDATIONS

It is recommended that the Environmental Protection Agency:

- Support a program to measure optical indices of common stack effluents. Data for a given type of effluent should be accumulated by a number of observers working at sites in different geographical locations to test the repeatability and universality of the measured indices. The best approach to index measurement may be to work with a classifier whose sized output is fed into an optical tester and monitored by a multiwavelength transmissometer. With the size known, the indices can be adjusted to produce the observed size dependent results.

- Develop a compact, "on-board" minicomputer to do real time data processing. The system can be functionally quite simple but should be capable of storing and rapidly addressing tables of data. The readout rate should be about 1/sec.

SECTION 4

FUNDAMENTAL CONSIDERATIONS AND GENERAL BACKGROUND

SCATTERING THEORY

Since the advent of the Mie scattering theory, it has been known that the scattering properties of a uniform spherical particle could be completely determined by specifying the complex optical index of the particle, the index of the surrounding medium, the radius of the particle, and the wavelength of the incident radiation. The extension to a size distribution of such particles is immediately obvious if each particle is treated as an independent scatterer. Recent experimental work (1,2) has shown that the volume (or mass) scattering coefficient for a polydisperse system of irregular but randomly oriented particles shows a remarkable similarity to the corresponding scattering coefficient for spherical particles. These results strongly suggest that even the irregularly shaped somewhat indescribable conglomerations normally found in stacks can be treated as if they were spheres because of the simplifying effects brought about by the statistical nature of the problem. Thus, if an index of refraction can be determined for the system and the particle size can be expressed by a reasonable distributional form, the optical effects caused by the system can be calculated.

The problem that is encountered in optical diagnostics is the inverse of the problem solved by Mie in that one or more characteristics of the scattering function are measured and the input parameters leading to them must be deduced. The question therefore is, that given the index of refraction, can the particle size be determined from measurements of such optical effects as the wavelength dependence of opacity. It is relatively easy to see that this is true for a single monodisperse distribution as a subsequent example will demonstrate. It is equally true, but not as obvious, for a size distribution that can be completely specified with a few parameters such as the mean and the standard deviation. It is probably untrue if the distribution is completely unspecified since there will be an infinite number of ways that a finite number of observed results can be created. It is most fortunate that natural processes tend to give rise to simple results. Many of the particulate systems can be described by the exceedingly simple log normal distribution while others may have a simple bimodal form. We obtained the data shown in Figure 1 by sampling the stack effluents of a cement plant with a cascade impacter. As plotted, a log normal distribution produces a straight line. More complex distributions would have to be approximated by a simplifying mathematical form.

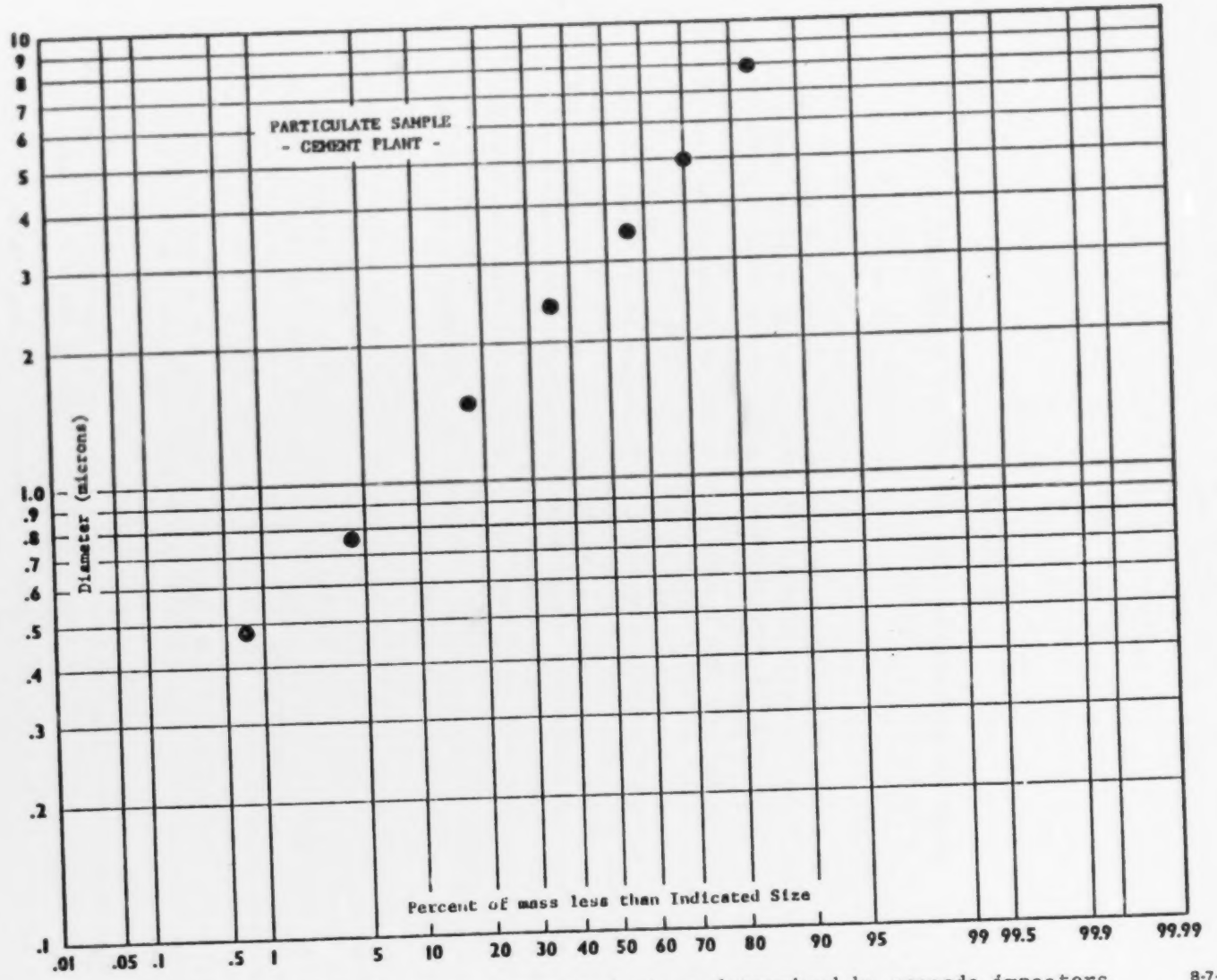

Figure 1. Size distribution of cement plant as determined by cascade impacters. 8-7-2-1

The principle on which an optical system might operate can be illustrated through a very simple example using a monodisperse distribution of water droplets and making the further simplification that the refractive index does not vary with wavelength. The relations of interest are as follows:

$$K(\lambda) = N_o\, Q(r, \lambda)\pi\, r^2 \qquad (1)$$

$$M_c = N_o\, \rho\, 4/3\, \pi\, r^3 \qquad (2)$$

where $k(\lambda)$ is the wavelength dependence of the extinction, N_o is the number density of the particles, πr^2 is the geometric area of particles of radius r, and $Q\ (r, \lambda)$ is the extinction efficiency which can be determined from Mie theory when the complex index of refraction is known. The second equation relates M_c, the mass concentration, to the density of the particulate material, (ρ), and the volume of a particle $(4/3\ \pi r^3)$. If, for example, the particles were 2 microns in radius and $N_o = 10^{11}/m^3$, the resulting values of $K(\lambda)$ which would be experimentally measured are as shown as open circles in Figure 2 where the K's have been plotted as functions of $1/\lambda$. The blackened circles show the different signature generated by 1 micron particles (where N_o has been set at $4 \times 10^{11}/m^3$ to keep the total geometric area the same. Figure 3 shows the Q function plotted as a function of r/λ. Figure 4 shows the data sets from Figure 2 fitted to the curve of Figure 3. From the amount of translation that is required to achieve each fit, r and N_o can be determined, the abscissa displacement is r, the ordinate displacement is $N_o\pi r^2$.

Normally the particles are not all the same size but have to be described by a distribution. In that case, N_o is replaced by $n(r)dr$ and the right-hand side of Equations (1) and (2) have to be integrated over the distribution. The best fit is then determined through use of a computer and an algorithm by adjusting the key parameters of the distribution (generally the mean and the spread). Since the index of refraction varies with λ, each $K(\lambda)$ must be fitted to its appropriate Q function instead of using a single function as above.

RELATED PROBLEMS

This general concept has been studied for a number of years at Aeronutronic. Specific problem areas covering the nature of the particle size distribution found at typical industrial sites, the optical indices of the material, problems with gaseous components, and data processing have been investigated in great detail along with the engineering problems that had to be met in order to build a practical optical instrument. Because the nature of the problem does not lend itself to simple analysis, most of the answers have to be determined experimentally.

Field work has been done at more than eight different industrial sites where the particle size distributions were monitored by cascade impactor studies and samples extracted for further laboratory analysis. The most common distributional form encountered was the log normal distribution, although it sometimes showed signs of truncation due to the pollution control systems that were employed. When the effluent contains two different species, such

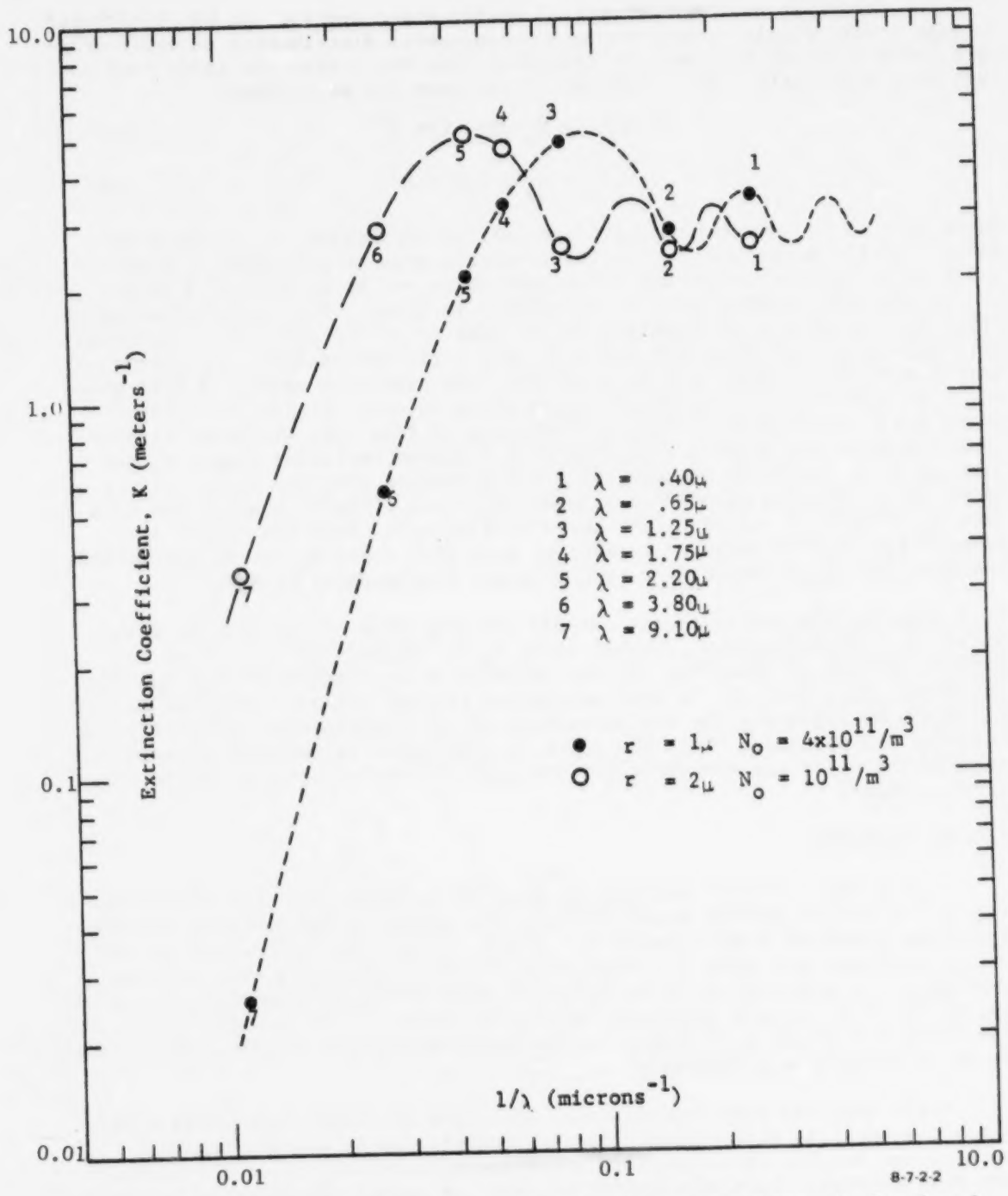

Figure 2. Experimental values of extinction coefficient, K, for 1 and 2 micron water droplets.

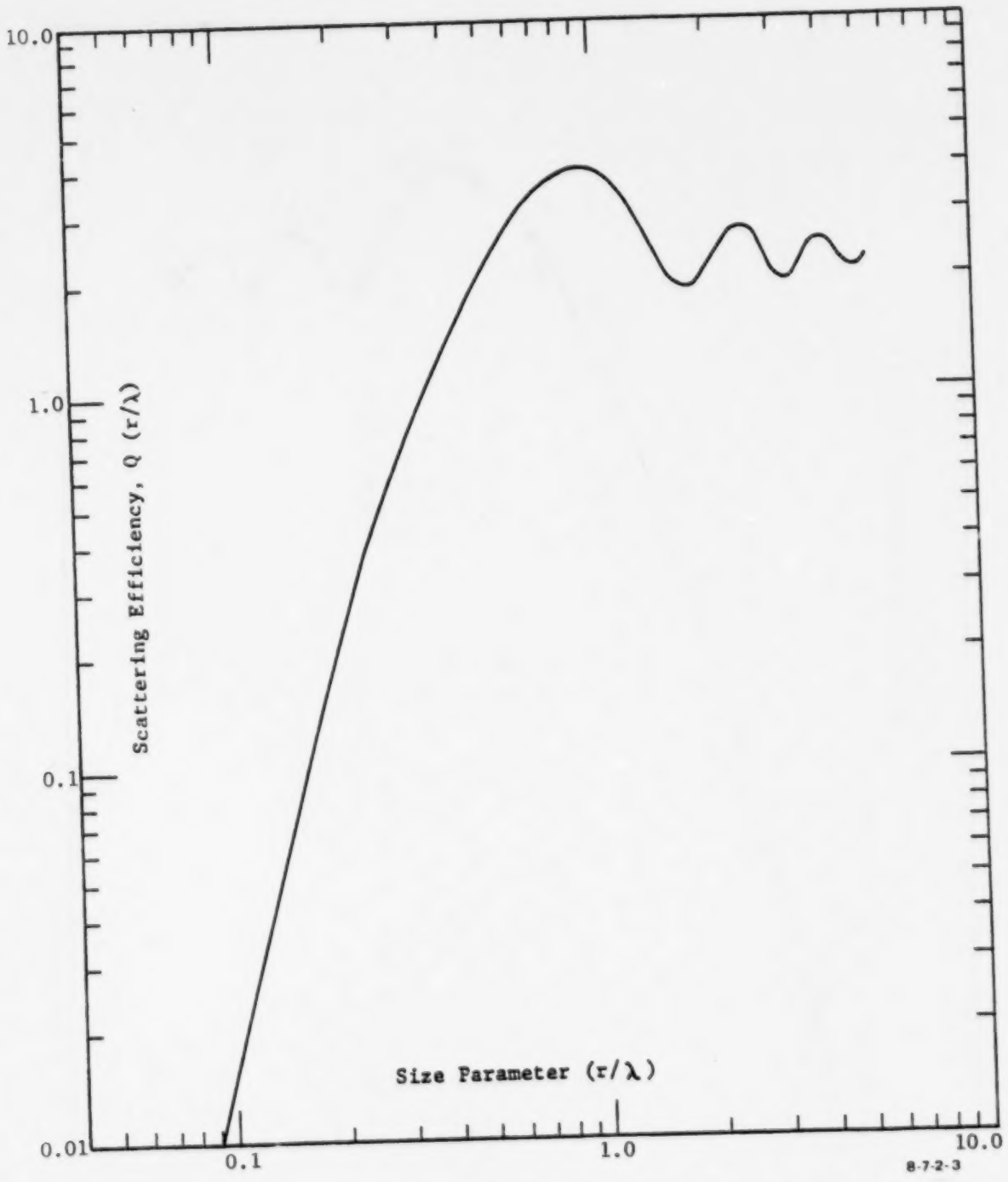

Figure 3. Dependence of scattering efficiency on size parameter for water droplets.

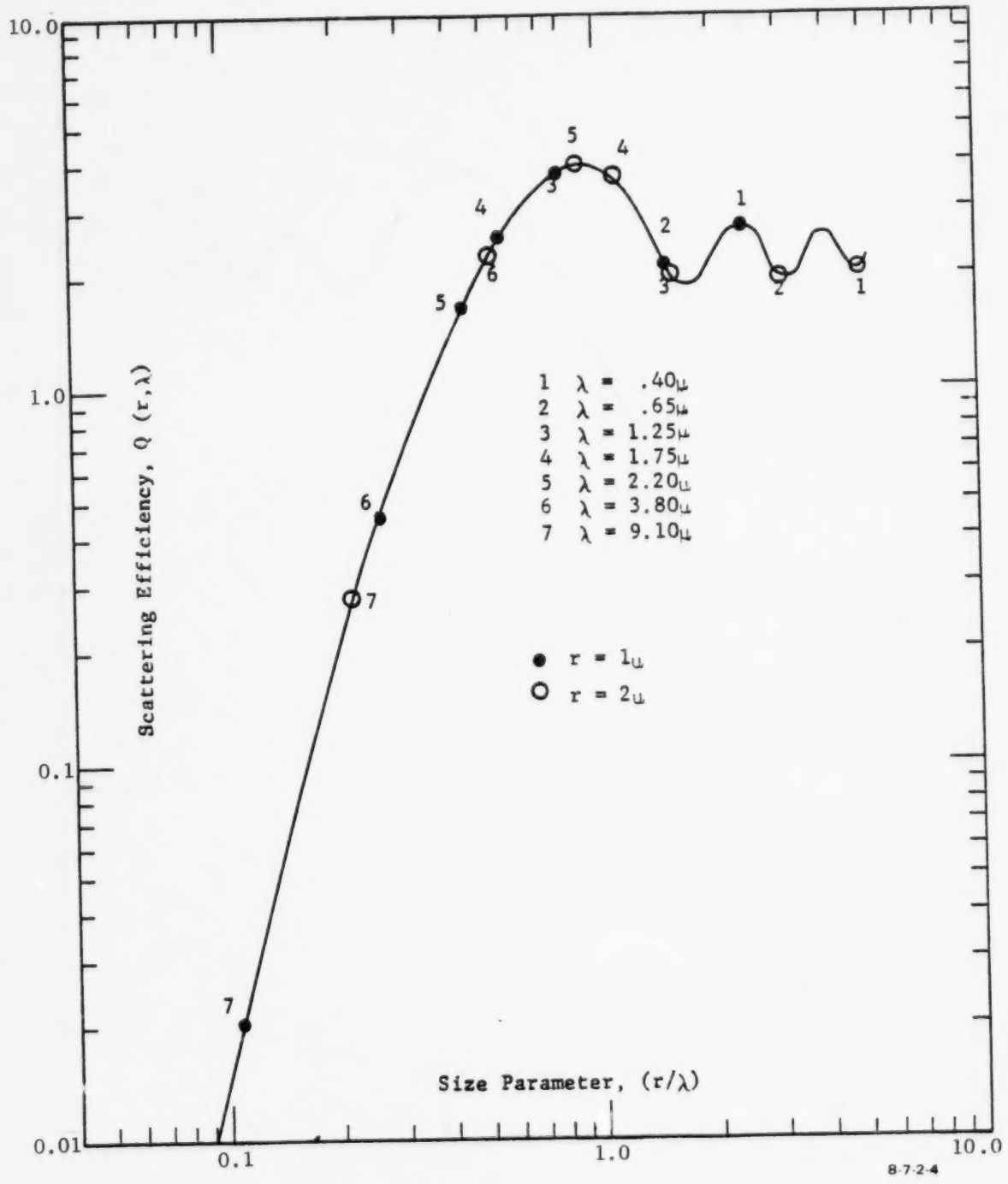

Figure 4. Experimental values of K versus $1/\lambda$ fitted to Q curve.

as soot and fly ash, there is generally a bimodal distribution. Whatever the form actually is, an approximation must be made that can be expressed mathematically so that it can be put into the algorithm. The computer program must then be able to fit the experimental data by adjusting size and shape parameters, defining the mathematical form of the distribution. Calculations of this type have been made with some of the data taken at the different sites. A breadboard version of a four wavelength single pass transmissometer was used to acquire this data.

It is unfortunate, but there is very little data available on optical indices. This appears to be true not only of the exotic stack particulates but also of the simplest materials we try to use as calibration particles. While the real part of the index may be known for many materials in the visible and the imaginary portions may be known for many materials in the infrared (IR), only a few materials have been completely studied. There are excellent data on water (3,4), ice (4), and quartz (5), and, more recently, data have been published on carbon (6)(results depend heavily on the type of source). Volz (7,8) has published data on atmospheric debris and esoterics such as ammonium sulfate, Sahara dust, volcanic dust, and debris from a coal-burning power plant. In prior study programs, if we categorized our sample as high in SiO_2 and resembling sand, we would use the index of quartz. If it was carbonaceous in form, one of the carbon curves would be used. Better data is needed to interpret results of the more sophisticated instruments that we are now constructing. Our plans for all current and future work include taking bulk samples of the particulates in question and making direct measurements of the indices of refraction using the technique presently employed by Volz.

The material being investigated is pressed into KBr wafers and the opacity of a known concentration is measured as a function of wavelength. This yields the imaginary part of the refractive index, n'. The material is also pressed into pellets which are polished for use in spectral reflection measurements. The real part of the refractive index, n, is calculated from the reflectivity equation.

$$r = \frac{(n-1)^2 + n'^2}{(n+1)^2 + n'^2}$$

The technique appears to be limited by the quality of the surface obtainable in the pellets, particularly for the shorter wavelengths. An alternate approach in the visible and near IR is to directly index match the particles with a working fluid. The fluid should be a mixture of two miscible liquids, one whose indices are lower than the particulates and one whose indices are higher. The indices of the liquids are determined by measuring the refraction at a given wavelength, using a thin liquid prism and Snell's law.

The index of the particulate is determined by finding the liquid ratio that minimizes the opacity of a liquid cell in which a specific concentration of the particulate has been suspended. The index matching must be done at all wavelengths of interest. Obviously, the particles must not react either physically or chemically with the immersion fluid.

The gaseous constituents in the stacks can also contribute to the measured opacity. If each operational wavelength is not selected with extreme care, a gas species might provide a major share of the opacity. It is not enough to know where the major windows are in the spectral absorption bands of the dominant gas species. In each window there are residual absorptions that arise from the tails of the major bands. Their contribution is a function of the partial pressure of the gas, the total pressure, and the temperature. An analysis of the residual absorption of CO_2, SO_2, and H_2O in the spectral window regions has been completed for two sites of interest. The work utilized an Aeronutronic computer program that, for a given wavelength, sums the absorption in the tails of all known absorption lines. The program then integrates these results for the filter bandwidth under consideration. The calculations were done using the gas parameters determined at two sites. The results are summarized in Table 1.

The residual absorption must be treated as corrections to the total measured opacities and the fluctuation in the residuals accepted as errors unless an independent effort is made to monitor the gas characteristics.

The problem of data processing is far more complicated than the sample curve fitting example given earlier. As previously indicated, there is generally a separate Q-curve for each wavelength and, therefore, completely separate integrals for each wavelength. The integrals are compared to the extinction coefficients being monitored to obtain estimators of N_o (one at each wavelength). If everything worked perfectly, the proper distribution function would result in all values of N_o being the same. In practice, a least square fit is done on N_o and the search is for the distributional parameters that minimize the residuals of the least square's fit.

The program can be made to minimize the influence of residual opacity due to gaseous absorption. This is done by subtracting out the average gaseous opacity from that measured. The effect of the variations in gaseous absorption are not important if the particulate concentration is high but can produce errors at very low levels of particulate concentration.

The earliest versions of a multiwavelength transmissometer employed single-pass optics with the detectors on the opposite side of the stack from the light source. While a system of this type can monitor either particle size or mass concentration, it is subject to a number of operational complications in that it cannot handle gain changes or zero drifts in the electronics and has no way of sensing changes in source brightness or the increased opacity caused by degradation of the optical components. The simplest way to overcome these shortcomings is to utilize a retroreflector-system on the far side of the stack and keep all other system components on one side. It is then simple to create a reference beam that can be distinguished from the primary beam in a number of ways (i.e., chopping frequency, time of occurrence, etc.). If this reference beam utilizes the same detectors and amplifiers that the primary beam does and most of the optics are common, then the system can be made to stabilize the output of the reference channel, thereby ensuring stability to the signal channel.

TABLE 1. CALCULATED ABSORPTANCE BY GASES IN THE OPTICAL WINDOWS

		Power Plant T = 423 ± 4°K L = 1524 cm			Cement Plant T = 458°K L = 610 cm		
Band μ	Bandwidth %	CO_2 14 ± 1/2%	H_2O 9 ± 1/2%	SO_2 550 ppm ± 50	CO_2 ~17.5%	H_2O ~6%	SO_2 ~10 ppm
11.3	1.7	0.17 ± 0.015	0.913 ± 0.097	0	~0.08 ± 0.008	~0.3 ± 0.04	0
11.3	3.9	1.20 ± 0.11	1.11 ± 0.12	0	~0.60 ± 0.06	~0.4 ± 0.04	0
10.0	2.5	~2.0 ± 0.2	~1.0 ± 0.1	0	~1.0 ± 0.1	~0.4 ± 0.04	0
8.86	0.9	~0	~0.4	~43.	0	~0.13	~0.23
3.88	2.2	<0.5	~0.7	0	<0.3	~0.2	0
2.25	2.0	<0.2	<0.2	0	<0.1	<0.07	0
1.70	4.0	<0.1	<0.1	0	<0.05	<0.3	0
1.27	5.0	<0.1	<0.1	0	<0.05	<0.03	0
0.64	10.0	0	0	0	0	0	0
0.435	7.0	0	0	0	0	0	0

The last problem to be considered is the mechanism by which the data is processed. The simplest system is to compare the incoming signal with a prepared nomograph that yields the size information. This technique was used during the early development of the system. With a little experience, it is possible to make useful deductions as to particle size by merely watching the output of the four channels. Our most recent system forms the data into a pulse code modulation for storage on audio tape. The tape is played into the main computer via a ground station normally used to introduce telemetry data to the computer. This was done because of the difficulty in introducing data into a major computer except via punched cards, etc. The problem is one of incompatible formats. With this arrangement, we were able to record 10 data sets per second which is far more than would normally be needed.

Recently, there have appeared on the market a number of data converters reported to have the ability of linking laboratory generated analog data directly to a major computer. The simplest solution to data processing is to build a microprocessor directly into the system. The output could be obtained in near real time in the form of a display or a printed record.

SECTION 5

THE TRANSMISSOMETER

GENERAL DESCRIPTION

The multiwavelength transmissometer is in reality four separate transmissometers, each operating at its own wavelength. The four channels use common mirror optics over most of the system and share a common path through the stack. Once the beam has returned to the receiver, it is broken down into four wavelength domains by a series of three beamsplitters which define four channels: the visible channel λ_1, the near IR, λ_2, the mid IR, λ_3 and the far IR, λ_4. The main splitter transmits in excess of 70 percent of the incident radiation throughout most of the visible and near IR. It reflects better than 80 percent of the incident radiation in the 4 to 13 micrometer range. In between, the splitting properties are not as good but, since the output of the source peaks in this range, there is more than enough energy. The transmitted light is further wavelength divided into visible and near IR by a splitter that reflects 95 percent of the incident radiation below 0.65 μ and transmits 90 percent above 0.75 μ while the reflected light is divided into mid-and far-IR by a splitter that reflects about 90 percent of the radiation below 4 μ and transmits better than 90 percent between 8 and 13 μ. The operational wavelength of each channel is precisely selected by means of a narrow band filter located within each of the four chromatic ranges. Each filter has been carefully selected to operate at a window of maximum transmission through the gas species normally found to stacks (i.e. H_2O, CO, CO_2, SO_2, etc.). Unfortunately, even in a window there is considerable residual absorption at elevated stack temperatures (i.e., a few percent). These residuals should be considered when interpreting transmissometer data, particularly when a particle concentration is low. Channel 1 operates at about 0.46 μ, Channel 2 at about 1.26 μ, Channel 3 at about 3.9 μ and Channel 4, a composite filter, at about 11.3 μ.

At the heart of the system are four detectors selected for their performance at the four wavelength regions: Channel 1 uses a silicon photodiode, Channel 2 uses a lead sulfide cell, Channel 3 is a lead selenide cell, while Channel 4 uses a broadband pyroelectric detector. The light that is measured by each detector is chopped at the source at 90 Hertz. A sync pickup is provided at the 90 Hz chopper in case it is desirable to monitor the signal us-

ing a phase locked amplifier. This sync signal is not currently used in data processing.

For about 90 seconds out of each 100 seconds, the beam passing through the stack returns to the detectors. For the remaining 10 seconds, a reference beam that never leaves the main unit impinges on the detectors. These two events are controlled by a chopper making one revolution every 100 seconds. The position of the chopper is monitored by two sync units, one which puts out a side pulse beginning before the beams switch from signal to reference and ending after they have switched back and the signal beam is restored. Thus no valid data is to be taken when the wide pulse is on. During the middle of the wide pulse, a narrow pulse is generated. It begins after the reference beam is fully on and ends before it begins to fade. Calibration is in effect only when the narrow pulse is on. The system is housed in four units. The largest unit is the transmitter/receiver package which contains most of the optics, the light source, the aforementioned beamsplitter and filters, the detectors, and their preamplifiers. The unit is 67.3 cm high, 52.1 cm wide and 14.6 cm deep (26½ in. x 20½ in. 5 3/4 in.) and weighs about 30.9 kg (67.9 lbs). It is designed for stack mounting and has been weatherproofed and ruggedized. The second unit, a retrosystem, is much smaller but similarly packaged. It is 49.5 cm high 26 cm wide and 13.3 cm deep (19½ in. x 10¼ in. x 5 ¼ in.) and weighs about 9.1 kg (20.1 lbs).

Figure 5 is a photograph showing main unit completely assembled while Figure 6 is a photograph of a unit with the cover removed showing the interior. Similar views of the retro-unit are shown in Figure 7 and Figure 8.

The optical system for the multiwavelength transmissometer was designed to maximize system efficiency and stability while minimizing system complexity and cost. Common optics were used wherever possible for both the signal and and reference beams. Since photodetectors, narrow bandpass filters, and dichroic beamsplitters are especially prone to variations in performance as a function of temperature, careful attention was given to making these components common to both beams to minimize thermally induced drift. The optical throughput of a beam is limited by two apertures. All other apertures are sufficiently overfilled or underfilled so that modulation will not occur due to a combination of edge effects and vibration or relative motion between conjugate or adjacent apertures. Mirror optics were employed throughout to eliminate variations between channels due to chromatic effects and to simplify the task of optical alignment. Wherever possible, stock components were utilized.

The final design was selected from a number of candidate systems. The transmitter/receiver units considered included using beamsplitters to combine and separate transmitter and receiver beams that share a common aperture and those that use essentially different portions of an aperture for the two functions. Retrosystems considered included a single element corner cube, a corner cube array, on and off axis cats-eye retroreflectors and on and off axis split-cats-eye retroreflectors. Since, under certain applications, the system might be energy limited, the most efficient design was selected, that using separate apertures and a split cats-eye retroreflector. The functional

Figure 5. Transmitter/receiver unit.

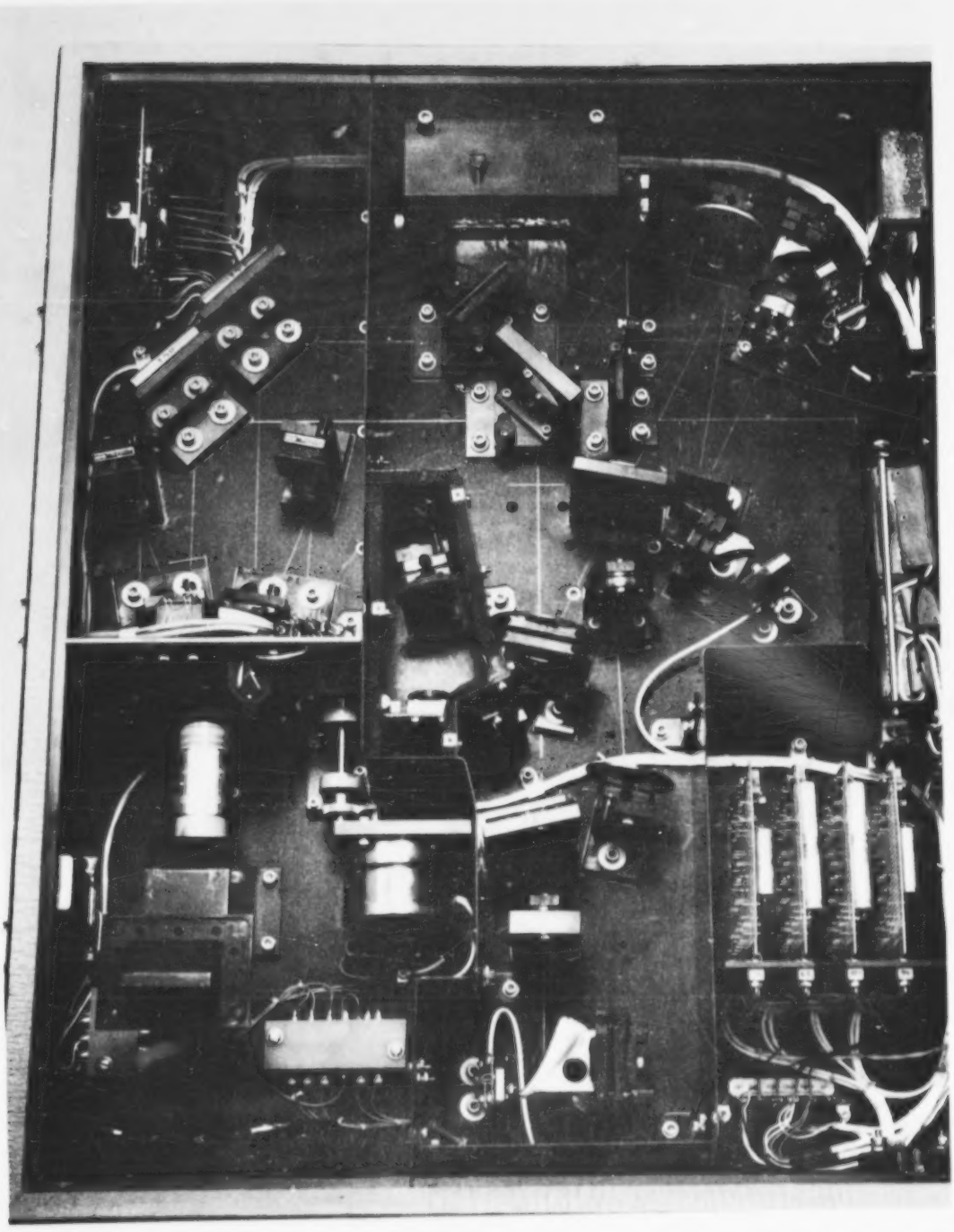

Figure 6. Transmitter/receiver unit (cover removed).

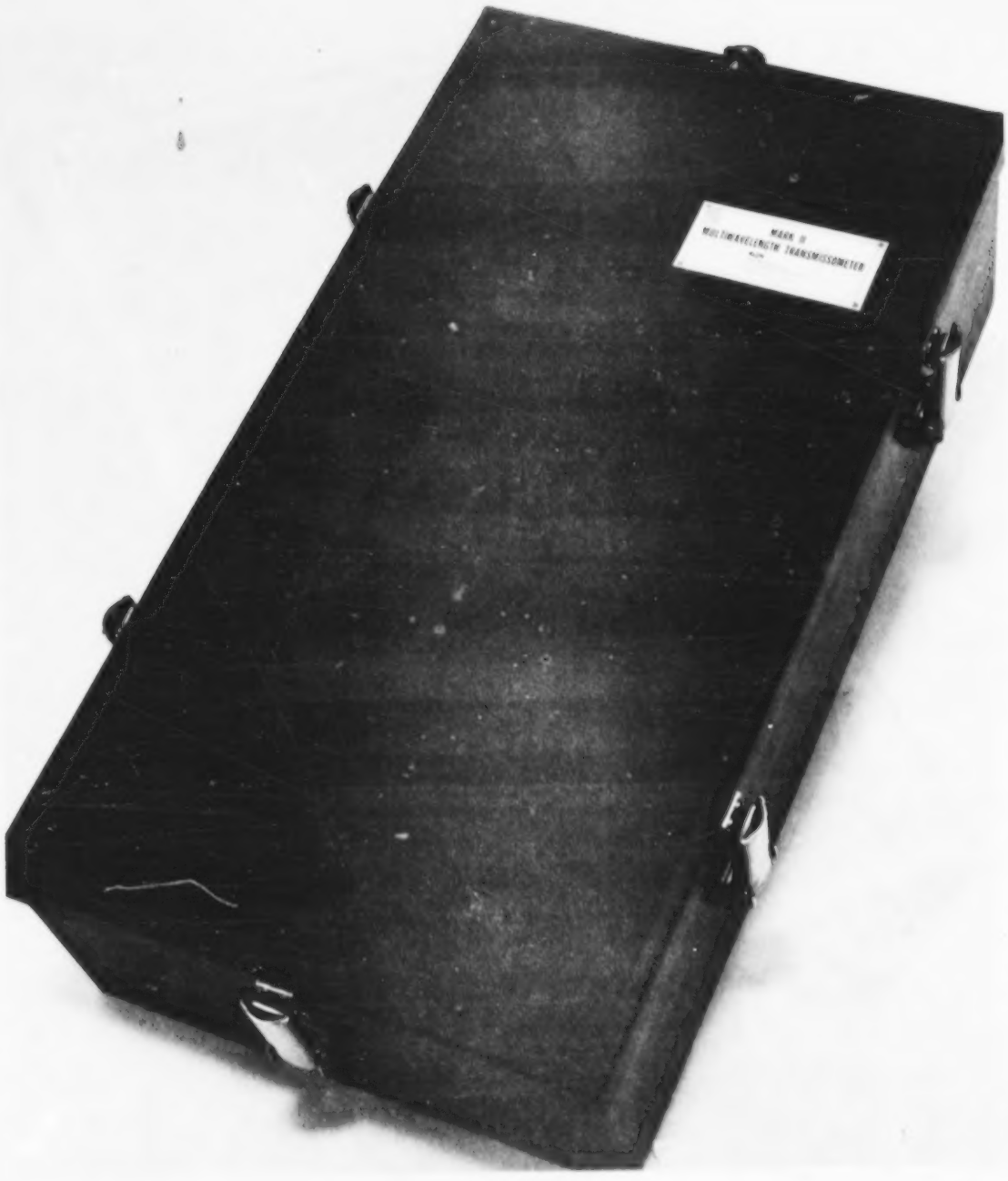

Figure 7. Retro-unit.

Figure 8. Retro-unit (cover removed)

details of the optical system are best demonstrated with the aid of an abridged schematic (Figure 9), illustrating only two channels. The transmitter and receiver beam have been deliberately crossed to minimize the effects of turbulence within the stack.

A Nernst glower source is imaged on apertures A1 and A8 by mirrors T1 and R1, respectively. A1 and A8 are similar in size and are overfilled by the images for stability. For the transmitted beam, A1 is imaged on C1 at the retro by mirrors T3 in combination with T4. For stability, C1 is smaller than the size of the image of A1. Modulation of the signal as a function of any angular motion or vibration of the transmitter is minimal and is limited to that and resulted from nonuniformities in the image that are caused by nonuniformities in the source radiant emittance and/or aberrations within the transmitter optics. Aperture A2 within the transmitter is imaged onto C2 within the retro by C1, and C1 is imaged onto C3 by C2. The image of A2 at C2 is imaged onto apertures A4 and A5 within the receiver by C3. Aperture A3 within the retro is almost conjugate to C1 and serves as a limit to the portion of C1 that is used. A4 is imaged onto photodetector D1 by S1. Similarly, A5 is imaged onto photodetector D2 by S4. The photodetectors are larger than the images. Apertures A4 and A5 are of equal size and are equidistant from dichroic beamsplitter F2. Narrow bandpass filters F4 and F5 are larger than A4 and A5 and are located near A4 and A5. Since A2 is conjugate to A4 and A5, and A2, A4, and A5 are all within the transmitter/receiver unit, there is no motion of the beam on A4 or A5 due to angular vibration of either the transmitter/receiver unit or of the retro unit. Placing the bandpass filters at these locations and making the photodetectors conjugate to them minimizes modulation of the signal that could occur due to vibrating these typically nonuniform components about within a probable nonuniform beam. Apertures A4 and A5 are slightly overfilled by the image of A2. The limiting apertures that define the throughput of the signal beam are A4 (A5) and A3. Within limits, angular motion or vibration of the retro unit will not modulate the beam as long as the image of A2 remains on C2 and as long as C2 is kept free of dirt or scratches. The angular motion of the retro must be restricted such that vignetting does not occur from the retro window W2 or from the sides of the path in the stack at either A3 or at the image of A3 or C1. A more detailed schematic of the retroreflector unit is presented in Figure 10.

For the reference beam, the source is imaged on and overfills aperture A8. Spherical mirrors R3 in combination with R4 form virtual image of A8 approximately the same distance from R4 as the retro is from T3. Radiant energy from R4 impinges on A4 and A5 with the same divergence as radiant energy from the retro unit. The beam is almost collimated. Aperture A9 is smaller than apertures A4 and A5 and the reference beam slightly underfills these apertures. Apertures A8 and A9 define the throughput of the reference beam. The diameter of aperture A9 was selected to make the outputs of the photodetectors about equal from the signal and the reference beams when the system was used on a 6 to 10 meter diameter stack. The reference beam is made coaxial to and coincident with the signal beam by beamsplitter R5. This beamsplitter is an uncoated BaF_2 window that results in little attenuation of the signal beam. The calibration chopper alternately transmits the signal and the reference beams to R5. Common areas of common optics are used for

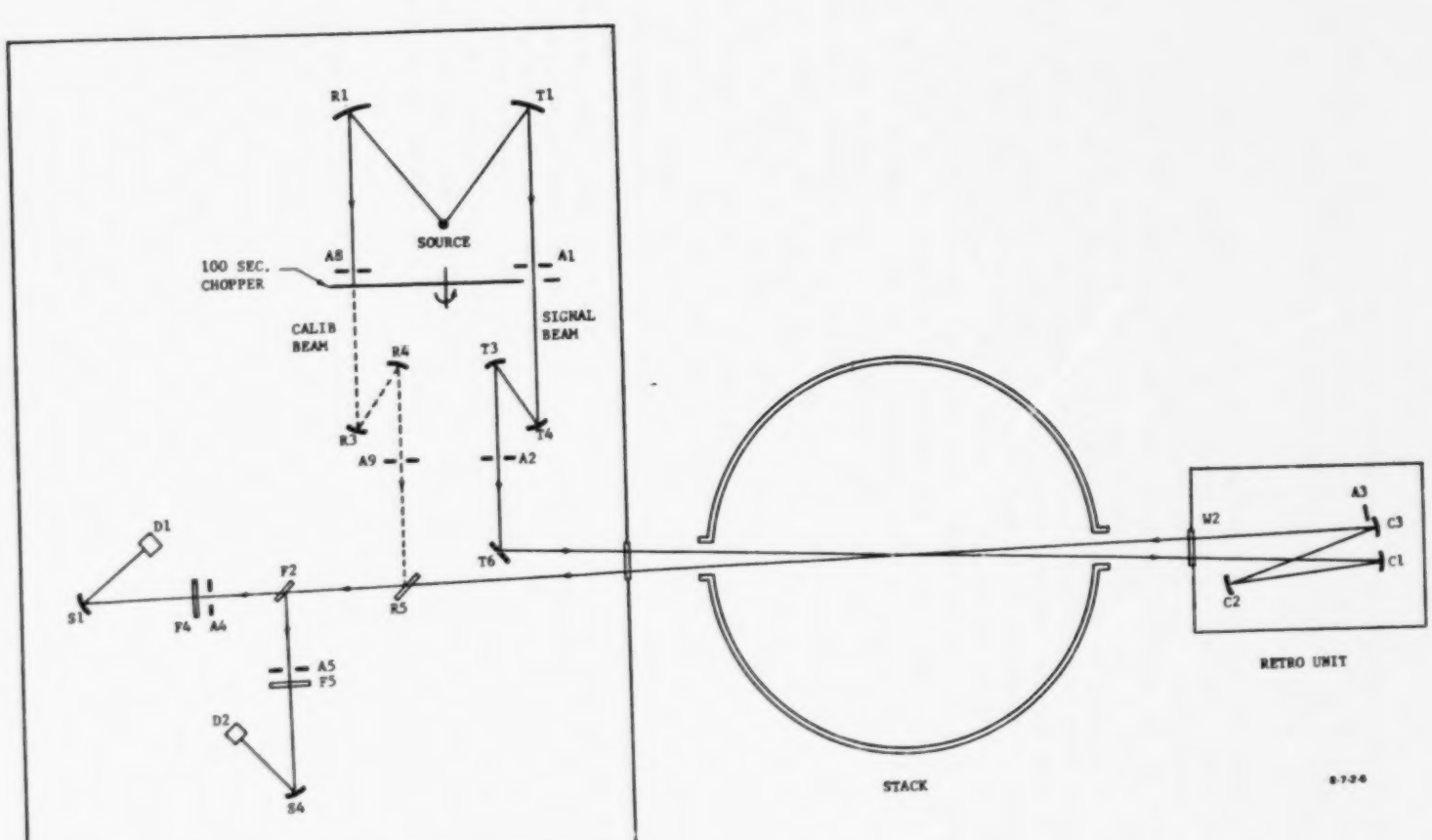

Figure 9. Schematic illustration of two spectral channels of the Multiwavelength Transmissometer.

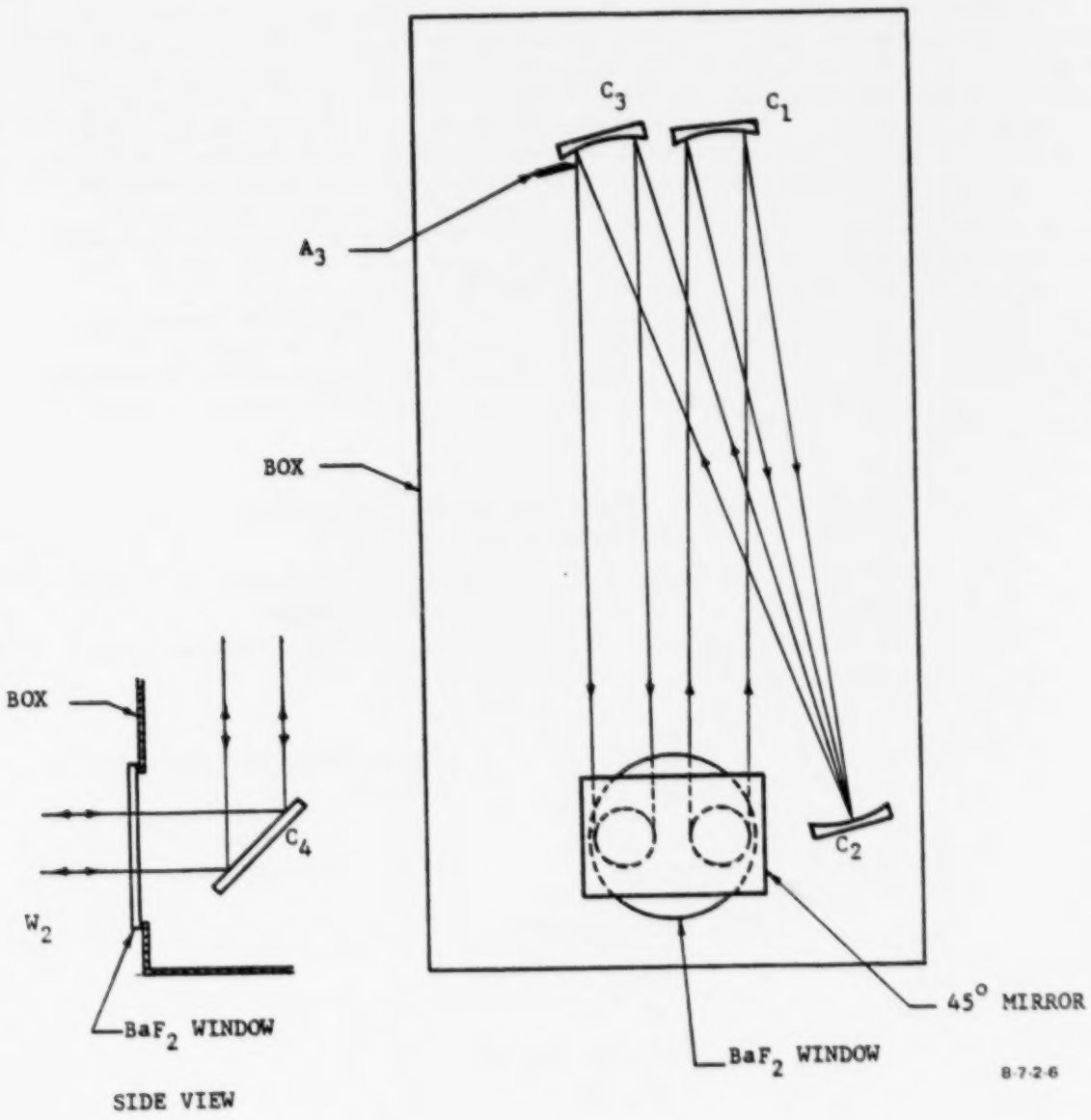

Figure 10. Split-cats-eye retroreflector unit.

both the reference and the signal beams after the two beams are combined at R5. This minimizes system errors that could arise from occurrences such as variations in the spectral transmittances of the filters or variations in photodetector outputs as the system temperature changes.

A detailed schematic diagram of the optics of the transmitter/receiver unit is presented in Figure 11. The nomenclature is the same as was used in Figure 9. Table 2 presents a list of conjugate points for the system. The general design and alignment philosophy was covered in the above discussion of Figures 9 and 10. Only deviations or additions are covered here. Photodetectors D1 and D2 have actually been made conjugate to a completely arbitrary point, i, set halfway between R5 and F1 rather than their respective apertures A4 and A5. This achieves the proper spot size at the detector while using off-the-shelf optical components and makes no significant difference in performance. Point i is essentially conjugate to A2 as are A4 and A5 because A4, A5 and point i are all almost equidistant from C3. F5 was placed at D2 rather than at A5 to help prevent stray light from saturating the detector. There is no significant image motion on F5 because it is essentially conjugate to point i. The spectral shift and bandpass broadening that results from placing F5 in convergent light does not adversely affect this channel.

TABLE 2. CONJUGATE POINTS FOR THE MULTIWAVELENGTH TRANSMISSOMETER OPTICS

Signal Beam	Reference Beam
Source	Source
A1	A8
C1	Virtual Image at Selected Distance
C3	
S8, S12, Crosshairs	S8, S12, Crosshairs

Signal Beam
A2
C2
A4, A5, A6, A7
D3, D4
Point i (Almost Conjugate to C2)
D1, D2

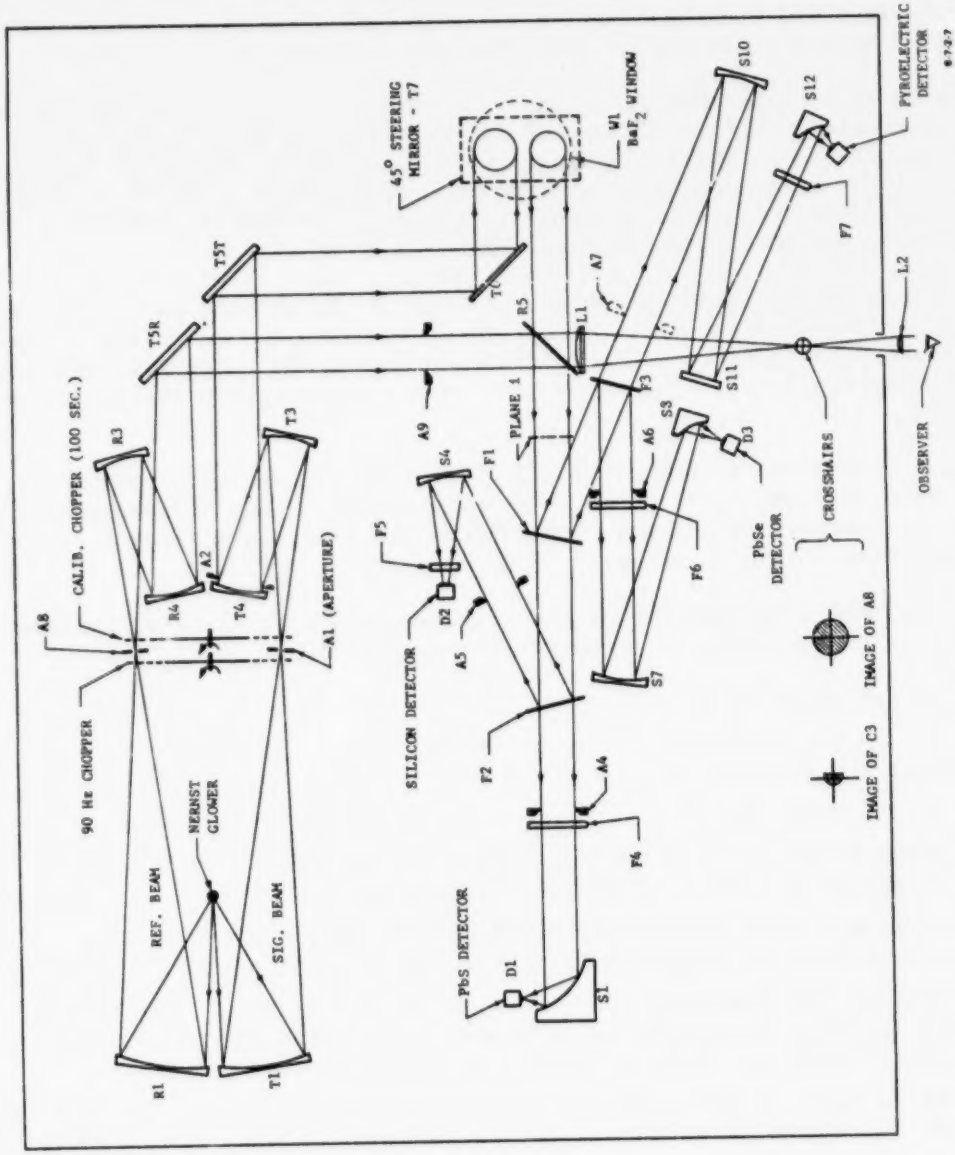

Figure 11. Schematic diagram of the transmitter/receiver unit.

Because the 11 μm channel was severely detector-noise limited, its aperture A7 was first made oversize then eventually eliminated and detector D4 serves as one of the two limiting apertures that defines the throughput for this channel. D4 is conjugate to the plane of A7. Filter F7 was moved relatively close to S12 to help block stray radiation to D4. These changes significantly improved the signal-to-noise ratio and resulted in no measurable degradation in the stability of this channel.

The built-in alignment telescope is comprised of lenses L1, L2, and a set of crosshairs. Either the signal or the reference beam can be viewed through the telescope while the system is in operation. Figure 11 includes a sketch of the reference beam image and the signal beam image as seen through the eyepiece when the system is properly aligned. Mirror T7 is adjusted to locate correctly the signal beam image.

It is necessary to adjust T6 and C3 when the instrument is shifted to stacks of different diameters. Mirror T6 is adjusted to center the transmitted beam on C1 and then C3 is adjusted to center the retroreflected beam on R5. These adjustments should be made before mounting the instrument on the stack.

While a complete alignment of all components is very time consuming, it need be done only once during the original assembly. Once the components in the receiver channel are located and aligned along with the telescope, they are permanently locked in place.

The following description of the alignment is an ideal case, perhaps best done only once prior to installation permanently on one stack.

- T3 and T4 focus A1 on C1.
- R3 and R4 create virtual image of A8 back the distance of C1.
- A2 is imaged on C2 by C1.
- Image of A2 at C2 is re-imaged by C3 to A4, etc. Some longitudinal motion of C2 will be required.
- Reference beam axis is reestablished by adjustment of T5 to center beam on telescope objective and crosshairs.
- Transmitter beam axes are reestablished by adjustments of T6 and C3 (perhaps C1 and C2) to restore all indicated ray paths and center beam on telescope objective (or A4) and crosshairs.
- T7 is used to re-aim output beam to accommodate flange inaccuracies on day-to-day deformations of stack and duct mounting configuration.

If an application calls for installing the system at many different locations, a series of compromises can be effected. This may cause minor reductions in signal but will not otherwise limit the performance of the instrument. Since typical stack diameters run from 10 to 30 feet, some median distance can be selected (i.e., 17 feet), thus,

- The reference channel can be set at -17 feet. R3, R4, and T5R can be permanently locked.
- The signal channel can be set at +17 feet. T3, T4, and T5 can be permanently locked.
- If the turbulence is not a limiting factor (it frequently is not), the system can be operated without a crossover, the outgoing beam striking C3 and then relayed back by C1. This enables T6, C1, C2, and C3 to be locked. The only adjustment will then be made by T7.

Under the above three simplifications, multistack operation is very straightforward. The complete adjustments will only need to be done when a stack is encountered with a diameter much smaller than the typical range (e.g., less than 5 feet).

ELECTRICAL SYSTEM

Of the four units comprising the transmissometer, one, the retroreflector, is completely passive in that it contains nothing electrical. The remaining three units are shown in Figure 12. The largest of these, the transmissometer itself, is internally wired in a manner illustrated in Figure 13. The 110 volt lines and similar power line are fed in from the Nernst Power Supply Unit by means of S04. A regulated -15 volts and +15 volts are fed in from the signal processing unit via S03. A relay actuated battery pack provides 135 volts dc for the ZnS and ZnSe detectors. The condition of the battery can be checked by pressing switch S1 and reading the voltage on meter, M1.

The outputs of the three sync pickups go to the sync pickup card mounted within the transmissometer box. The card circuitry is shown in Figure 14. The signals are clipped and then amplified. The wide sync signal is inverted by means of a second stage. The sync outputs terminate at BNC connectors on the connector panel of the transmitter box.

The outputs of the four detectors go to four preamplifier cards that are essentially the same for all channels. The differences that occur are in the input circuitry and the gain settings. The schematics of the preamp cards is shown in Figure 15; Channels 2 and 3 use battery operated photoconductive detectors that create a driving signal across R11. Channels 1 and 4 have their own preamplifiers with outputs directly across terminals 9 and 10 (R11, R12, and C7 are not needed). The potentiometer, R5, is used to balance the DC offset of the preamp. The gain of each channel is adjusted by selecting the value of R3 to produce a reference signal output of about 1.75 volts peak-to-peak. The chopped signals appear as square waves. The output of each channel terminates on the connector panel of the transmissometer box.

The remaining electrical units, the Nernst power supply box and the signal processing box, are designed for use in a control room environment and have not been ruggedized as have the optical units. They are shown in the form of a table mounted chassis in Figure 16 but could easily be adapted

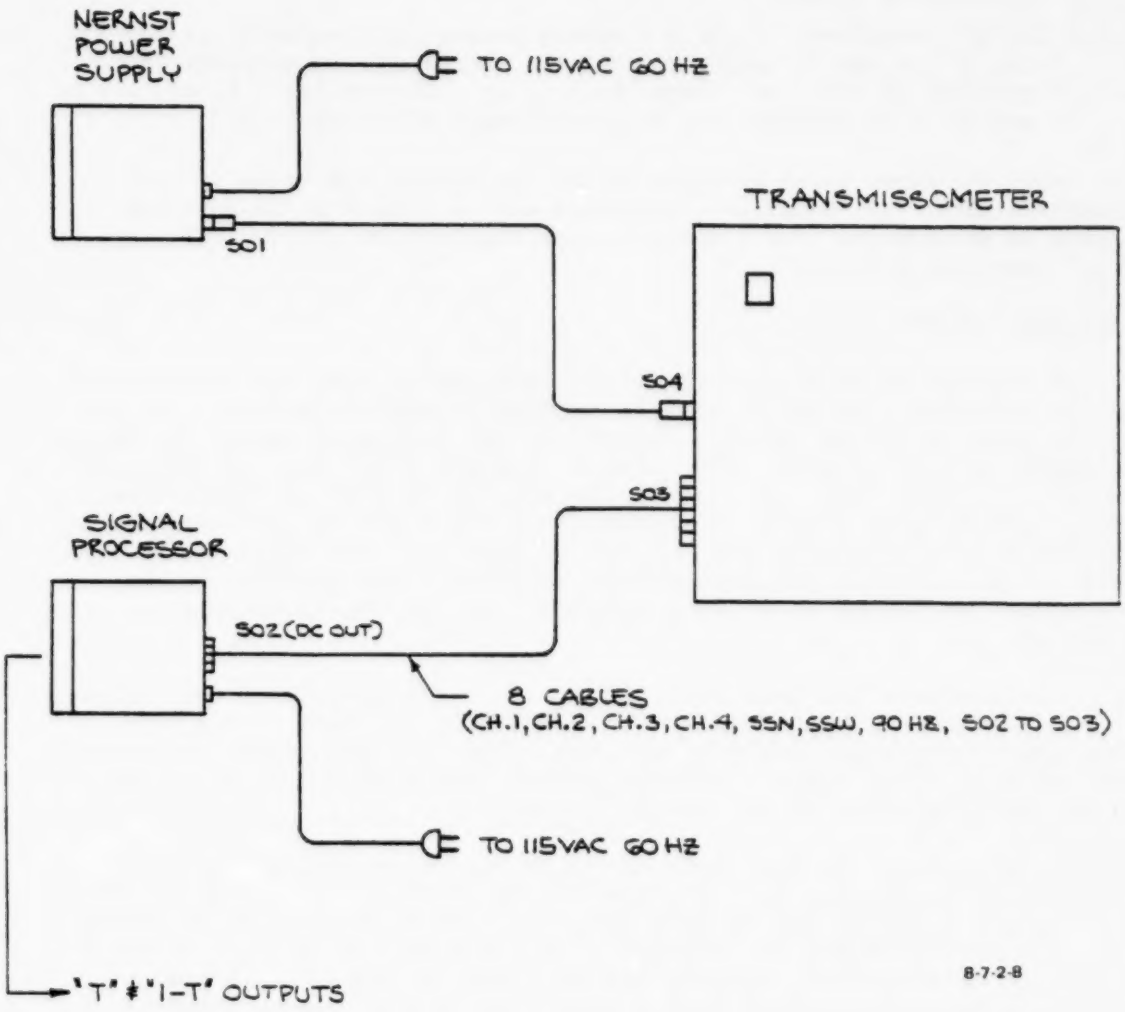

Figure 12. Electrical interconnections.

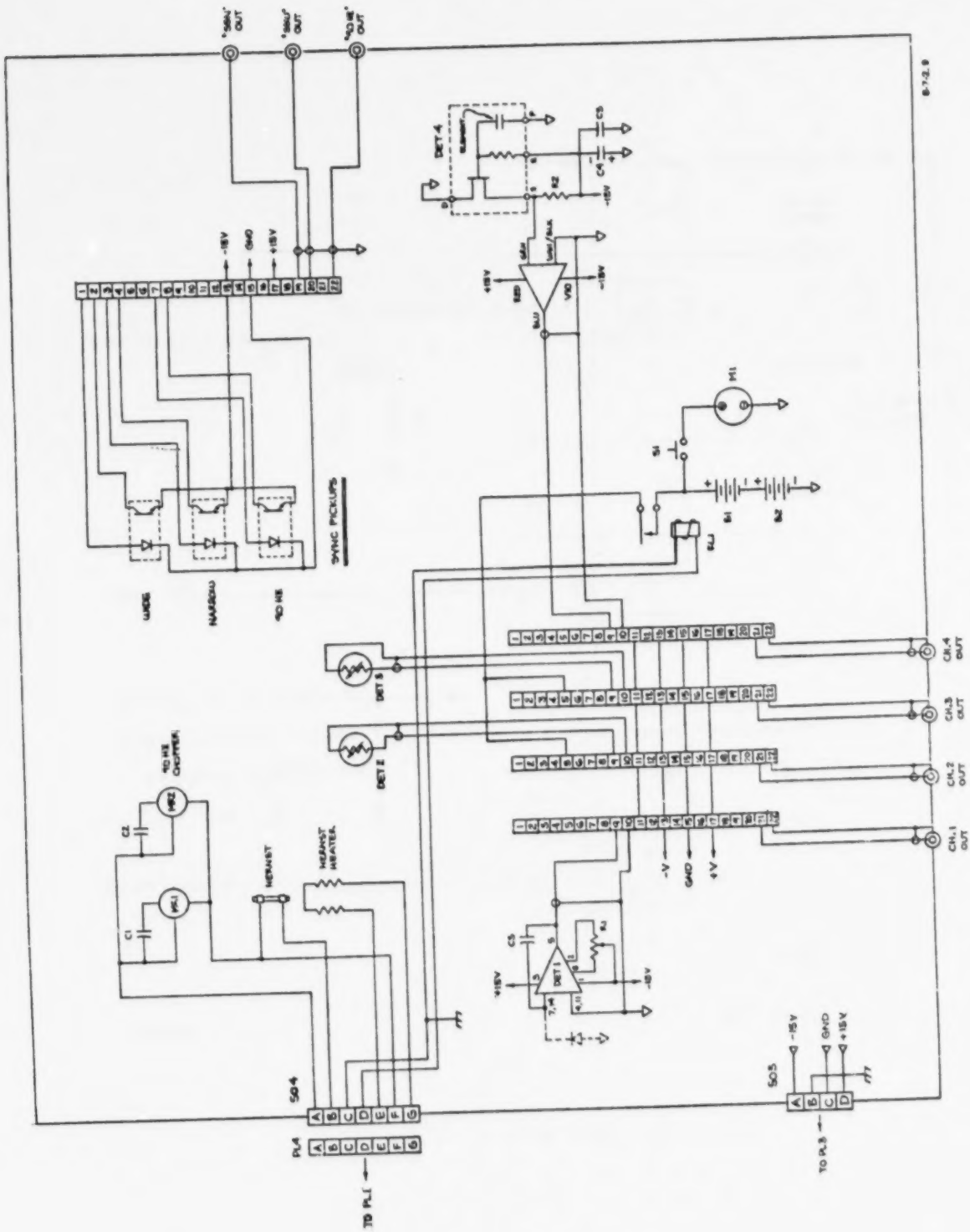

Figure 13. Transmitter/receiver wiring diagram.

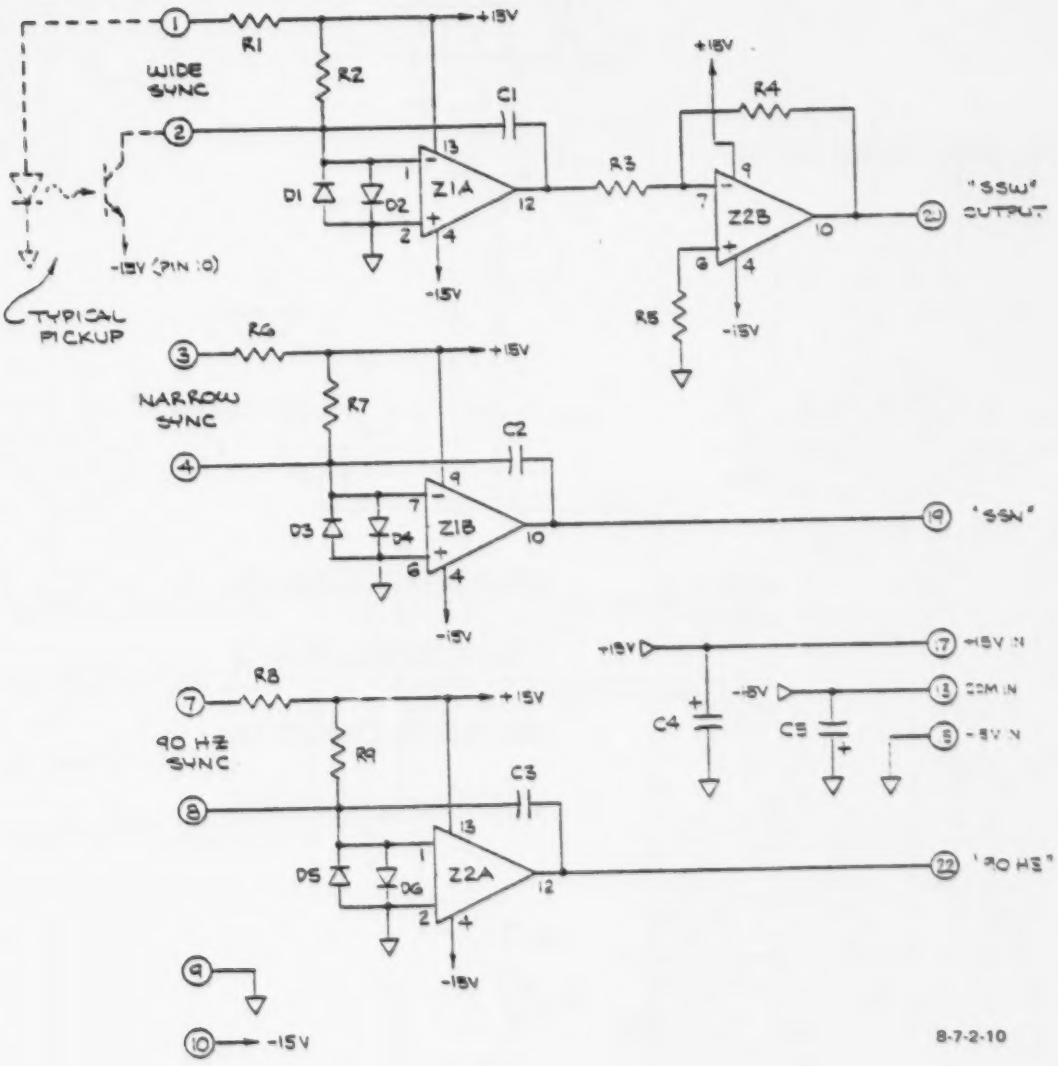

Figure 14. Sync pick-up schematic.

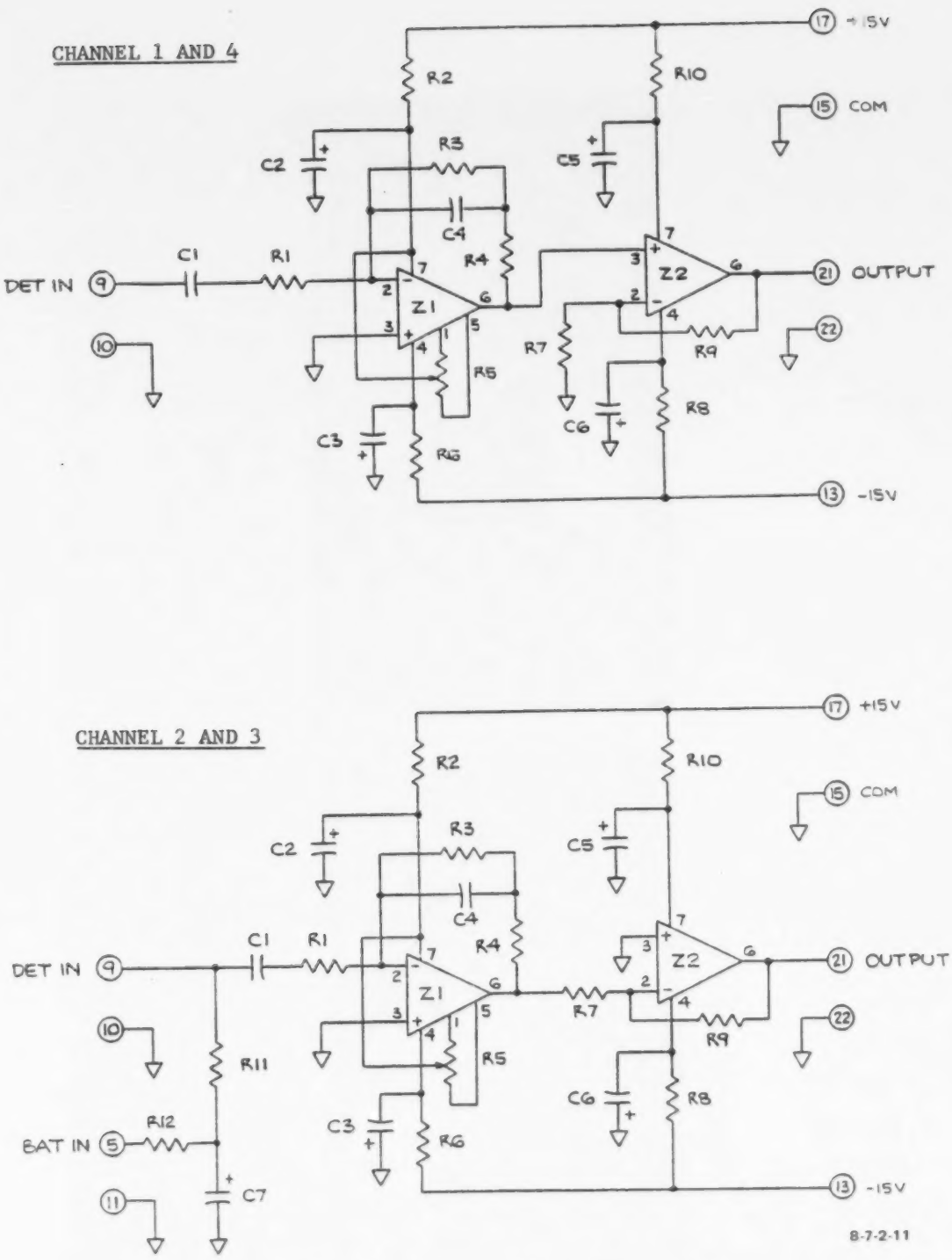

Figure 15. Preamplifier schematics.

Reproduced from
best available copy.

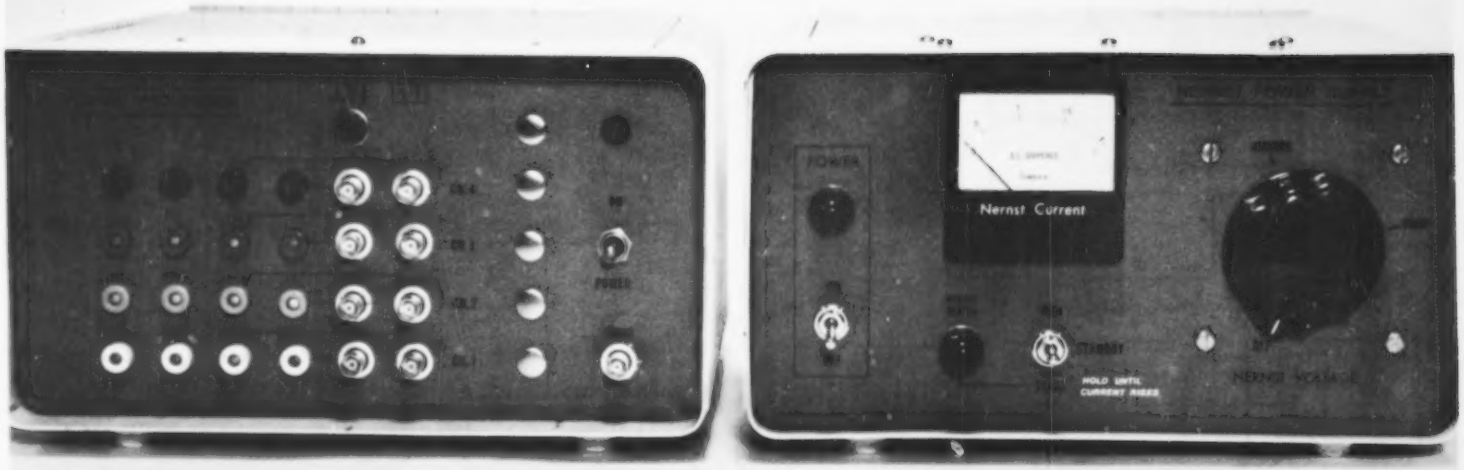

Figure 16. Electrical units.

for rack mounting. The internal view of the Nernst power supply box is shown in Figure 17 while the schematic is shown in Figure 18. A wiring diagram of this box is given in Figure 18. If the unit is to be inoperative for several days, it is desirable to keep the Nernst operating at a reduced power level; a standby mode is available. This minimizes both the thermal shock to the unit and prolongs its operational lifetime.

The main electronic functions are conducted in the signal processing box. It contains four AGC amplifier cards, a reference voltage card, and one $\pm$ 15 volt commercial dc supply. The reference voltage card, (Figure 19) has a $\pm$ 15 volt input, a regulated $\pm$ 12 volts output, and a 6.2 volt reference output.

The wide and narrow sync signals are amplified by the sync amplifier card - the circuitry of which is shown in Figure 20. The wide sync output is normally +15 volts swinging to -15 just prior to the switchover from signal to reference beam and returning to +15 volts soon after the return to the signal beam, an interval of about 10 seconds. The narrow sync signal is normally -15 volts and swings to +15 volts during the interval that the reference beam is on and steady. Calibration takes place during the interval when the narrow sync is positive, a period of about 5 seconds. A third voltage, picked off of the wide sync channel, is normally +5 volts but goes to zero volts when the wide sync goes to -15. This voltage appears at the event terminal and is used to tell a computer to ignore data during the 14-second interval when the signal beam will be interrupted. The timing sequence of the sync probes is illustrated in Figure 21.

The four AGC-amplifier cards are essentially identical. A typical circuit diagram is shown in Figure 22. The quasi-square wave signal from a given preamp card (i.e., channel 1) is fed into AGC - amplifier card number 1. The first stage, Z3A, and its associated components constitute a bandpass filter that convert the input square wave into a sine wave. The signal is attenuated by a factor of approximately 50/1 at the input of Z1A. The gain of Z1A can be varied between 50 and 300 depending on the state of Q1. When Q1 is open (in a high impedance state), the gain of Z1A is controlled by R6 and R24 and is about 50. When Q1 is closed (i.e., in a low impedance state), the gain is controlled by R6 in series with R23 and R24 in parallel. The gain is then about 300. Between the attenuator and the variable gain, the system produces an effective variable gain ranging between unity and six.

The output of Z1A is fed into a precision full wave averaging circuit composed of Z4A, Z3B, and their associated electronics. This output (Z4 pin 12) is a dc voltage equal to the average of the rectified sine wave at Z1 pin 10. This dc signal is fed back to the AGC loop through R32 to Z1B pin 1 where it is compared to an AGC reference voltage level set by potentiometer R20 and appearing on Z1B pin 2. The combination of Z1B, R32, and C11 serve as an integrator. Q3 is a switch feeding a sample and hold circuit composed of Z2, Q2, and C1. Since Q2 has a very high input impedance and Z2 has a very high output impedance, C10 is essentially isolated until Z2 is switched to a sample state by the narrow sync pulse. The output of Q2 which is coincident with the junction of R27 and R28 will reset itself to an updated value, hope-

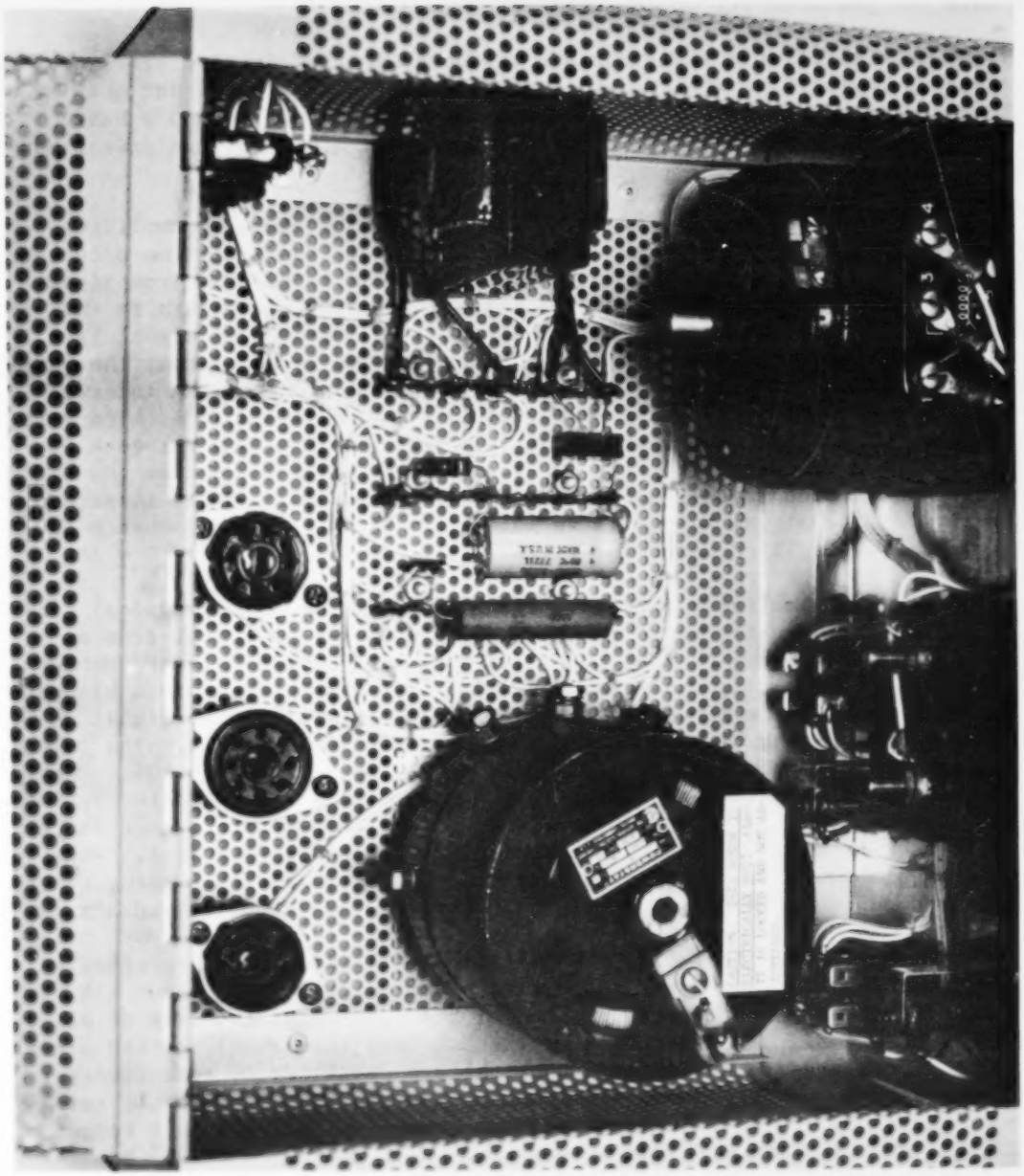

Figure 17. Interior of Nernst power supply unit.

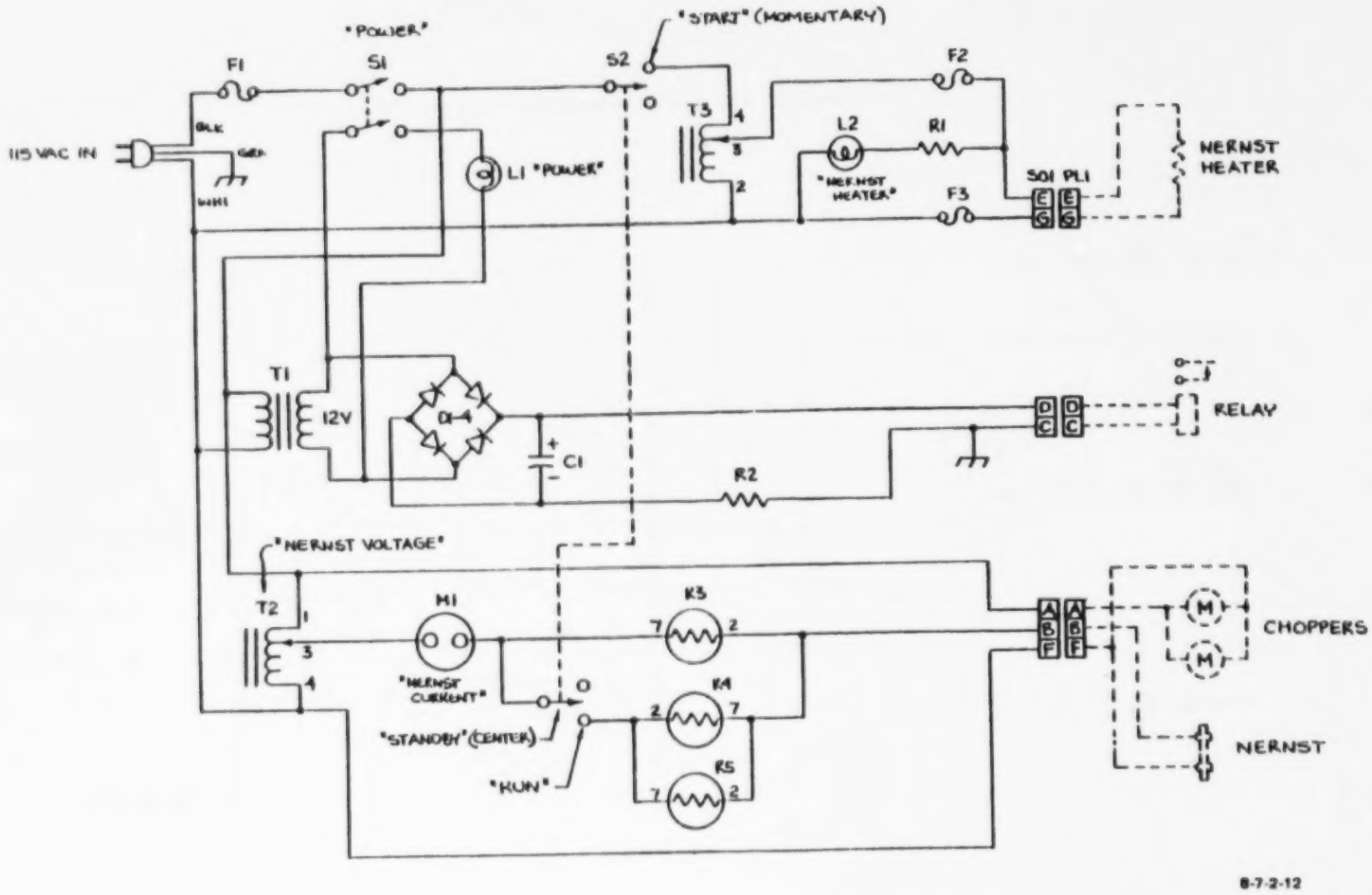

Figure 18. Nernst power supply schematic.

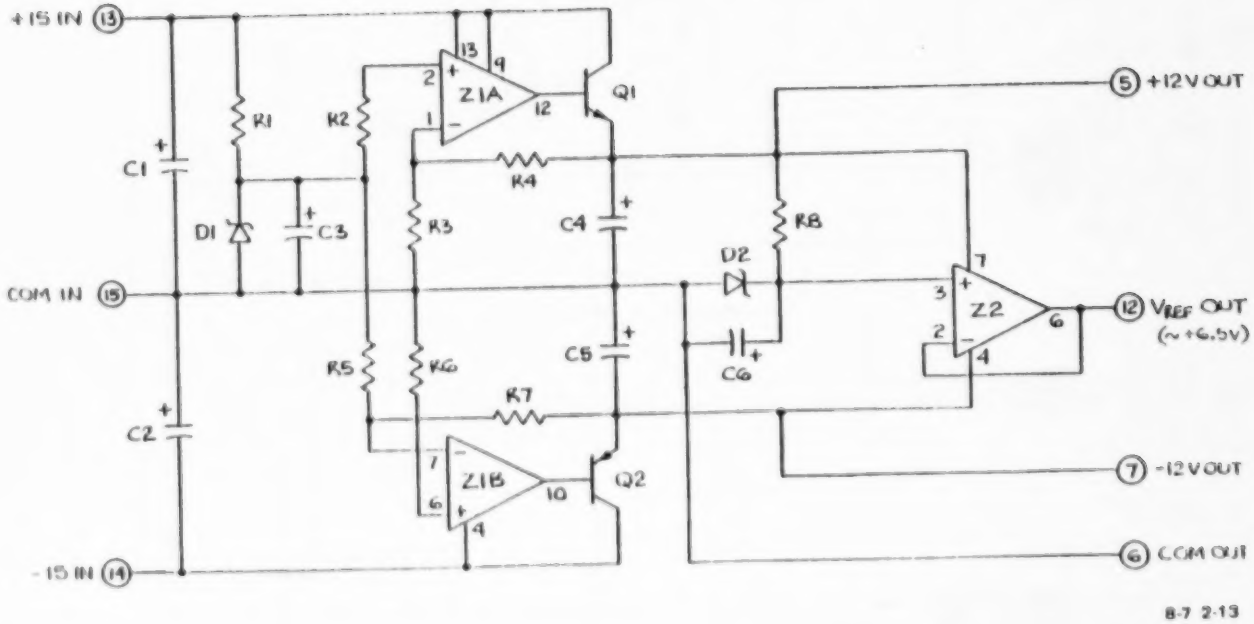

Figure 19. Reference voltage schematic.

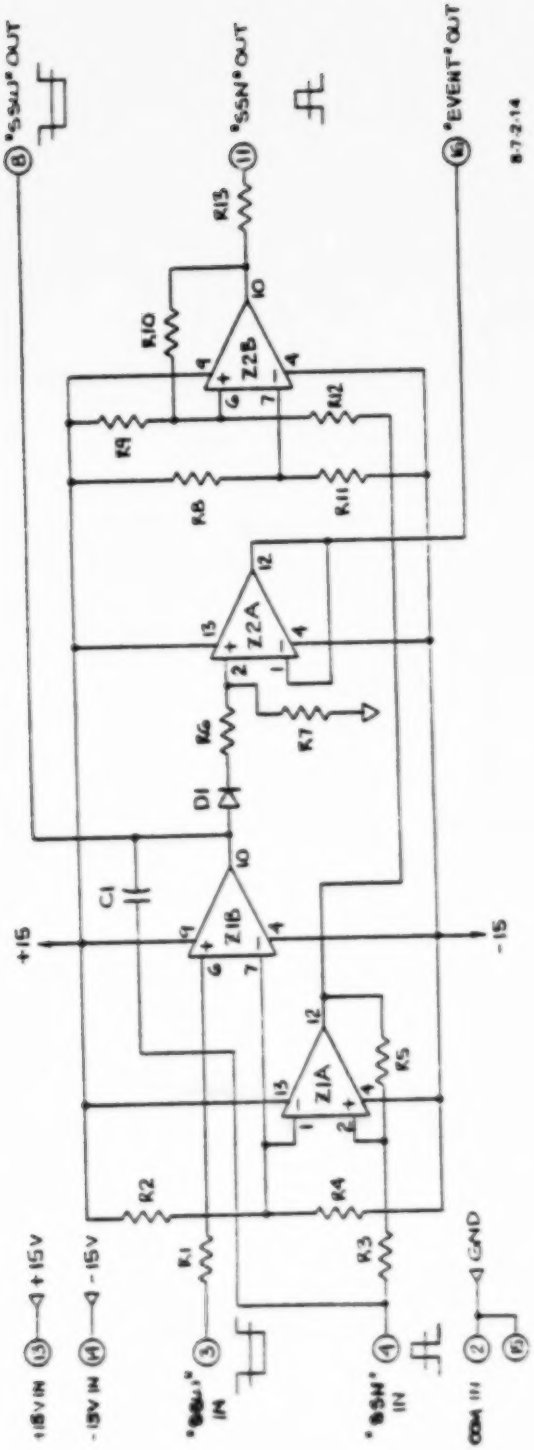

Figure 20. Sync amplifier schematic.

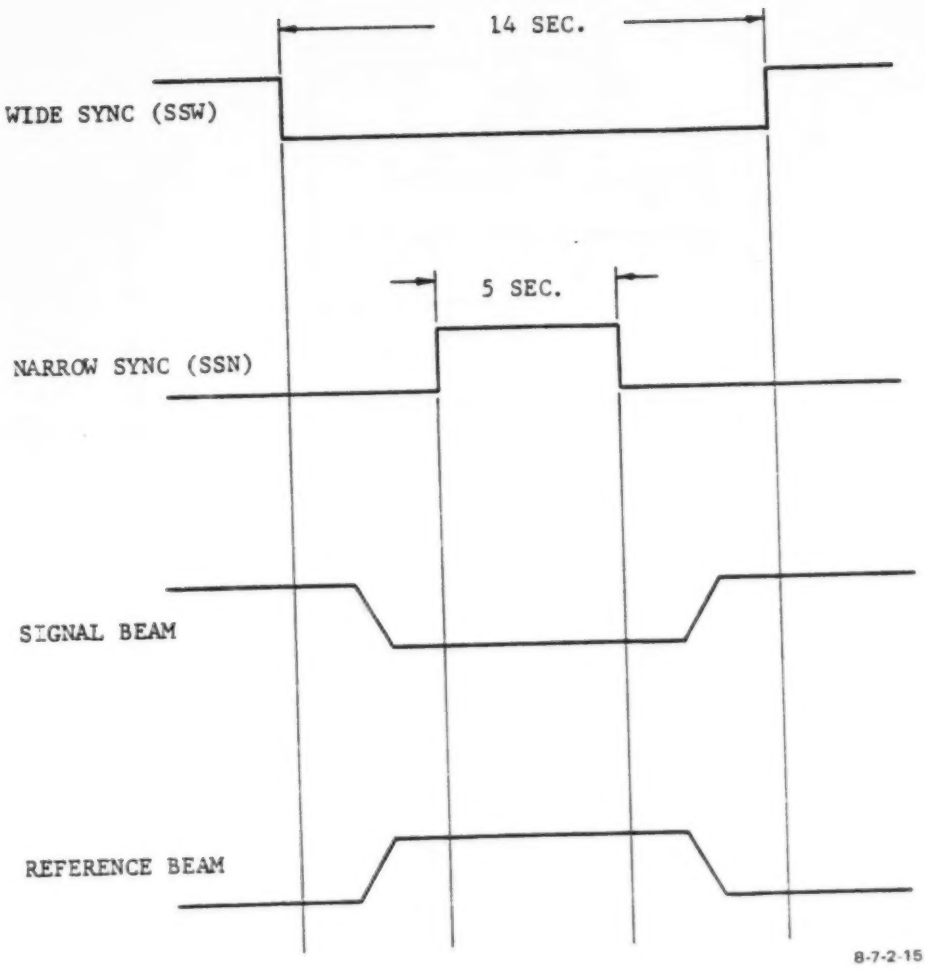

Figure 21. Sync timing sequence.

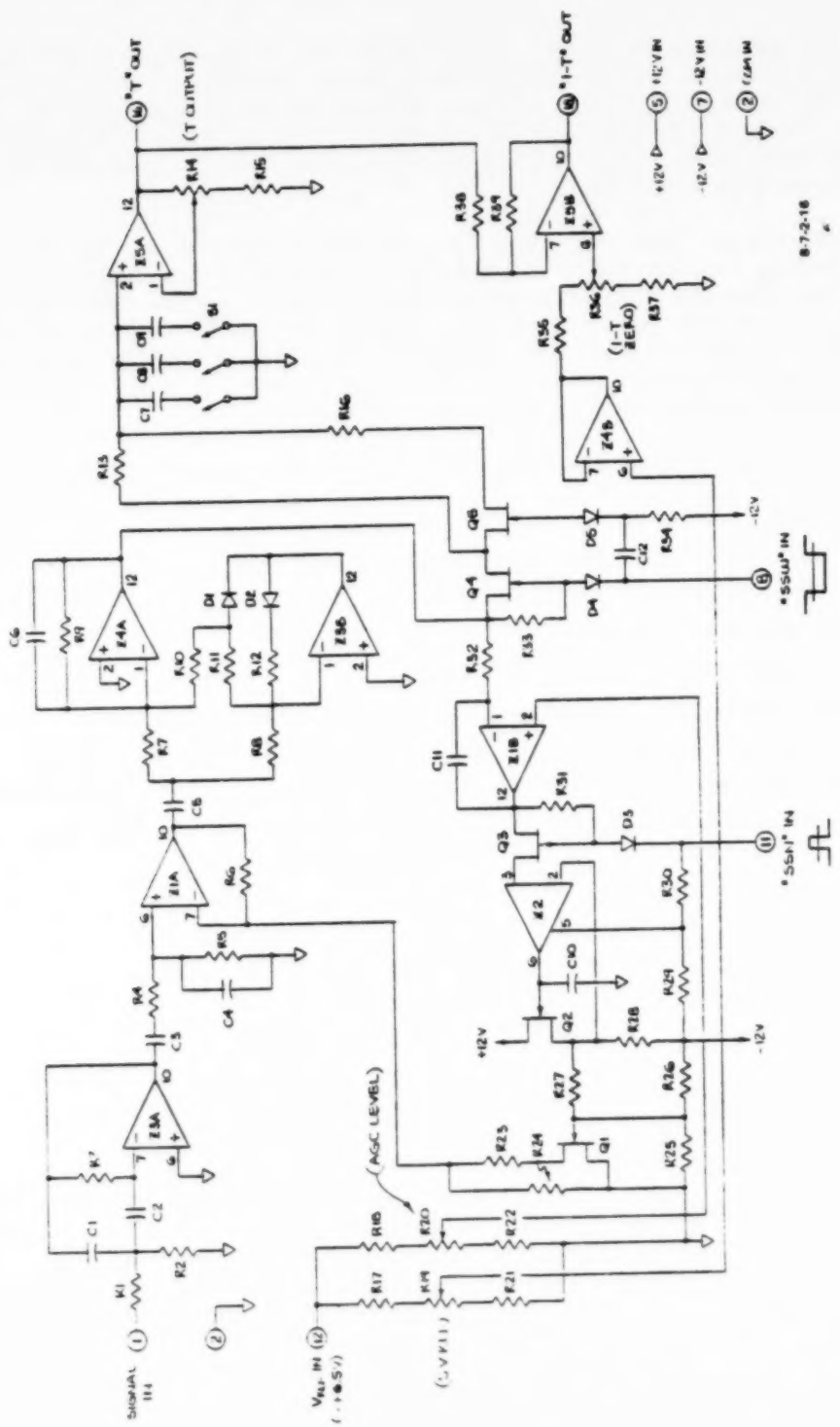

Figure 22. AGC amplifier schematic.

fully close to its previous value. This signal drives Q1 and sets its internal impedance somewhere between near zero to near infinite. This in turn sets the gain of Z1A between 300 and 50 (i.e., overall stage gain of 6 to 1). Thus, the AGC loop tries to set the gain of Z1A so that the dc signal caused by the reference beam (i.e., Z1B - pin 1) is equal to a preset precision voltage set by R20 at feed to Z1B - pin 2.

The signal output from Z4A - pin 12 goes to Z5A when Q4 is closed as it normally is during the operate portion of the 100-second duty cycle. The gain of Z5A has been adjusted with potentiometer R14 so that at 100 percent transmission, the signal level is exactly 5 volts at the "transmission out" terminal (i.e., "T" out). With "T" out set at 5 volts, R19 is adjusted so that "1-T" out is 10 volts. Thus, as "T" swings from 5 volts to 0 volt, the "1-T" output will swing from 0 volts to 10 volts.

A summary of the events that are involved calibration is as follows:

- Wide sync open Q4 ... Output "T" floats.
- Beam undergoes transition from signal to reference.
  ... reference signal established.
- Narrow sync on, closes Q3, allows AGC to reset.
- Narrow sync off, Q3 opens, AGC fixed.
- Reference beam off, signal beam on, signal beam stabilizes.
- Wide sync off, Q4 closes, Q5 momentarily closes for quick reset of voltages on C7, C8, and C9, the output time constant capacitors.
- Q5 opens restoring RC time constant (i.e., R13 and C7, C8, C9).

SECTION 6

LABORATORY STUDIES

DUST CHAMBER

The work described in this section was done as part of an ongoing Independent Research and Development program conducted by the Advanced Development Operation of the Ford Aerospace & Missile Systems Division. The multiwavelength transmissometer was conceived and developed during earlier phases of this technical effort. The current program involves testing the performance of the instrument in a controlled laboratory situation. The program and the results have been included in this report for the sake of completeness.

Under the program, it was necessary to develop a dust generating system that could be used to create particulate environments similar to those found on industrial stacks. The system, Figure 23, incorporates a system of blowers, sieves, and sieve shakers to disperse the powdered solid into an air stream. The particle ladened air has to traverse a series of baffles which serves to remove the agglomerates. The resulting aerosol is passed into a 2.7 cubic meter holding volume or dust chamber where any remaining oversize particles settle out during the more than 20-second residence time. The aerosol is diluted with clean air and then passed down a 0.2 meter diameter duct which acts as the optical path and, finally, the aerosol passes up and out through a roof exhaust fan. The optical path length can be adjusted from 1 to 10 meters. The flows in the system are governed by a series of dampers: one at the exit of the dust chamber which determines the amount of dust-laden air entering the optical path, one which regulates the amount of dilutent air, and one at the exhaust end which regulates the gas velocity in the optical chamber.

The concentration of the dust is controlled by varying the number of sieves, the mesh size, and the sieve area. It is also controlled by the amount of dilutent air that is mixed with dust-ladened air. Once the particulate has reached the optical chamber, it undergoes continuous optical monitoring and can also be sampled isokinetically as desired. One of the best sources of particulates are the effluents arising from the industrial sites of interest. The material is generally collected from the pollution control systems. The indices of refraction at the wavelengths of interest are measured using the techniques described in Section 4. This information serves both the lab experiments and possible future site experiments.

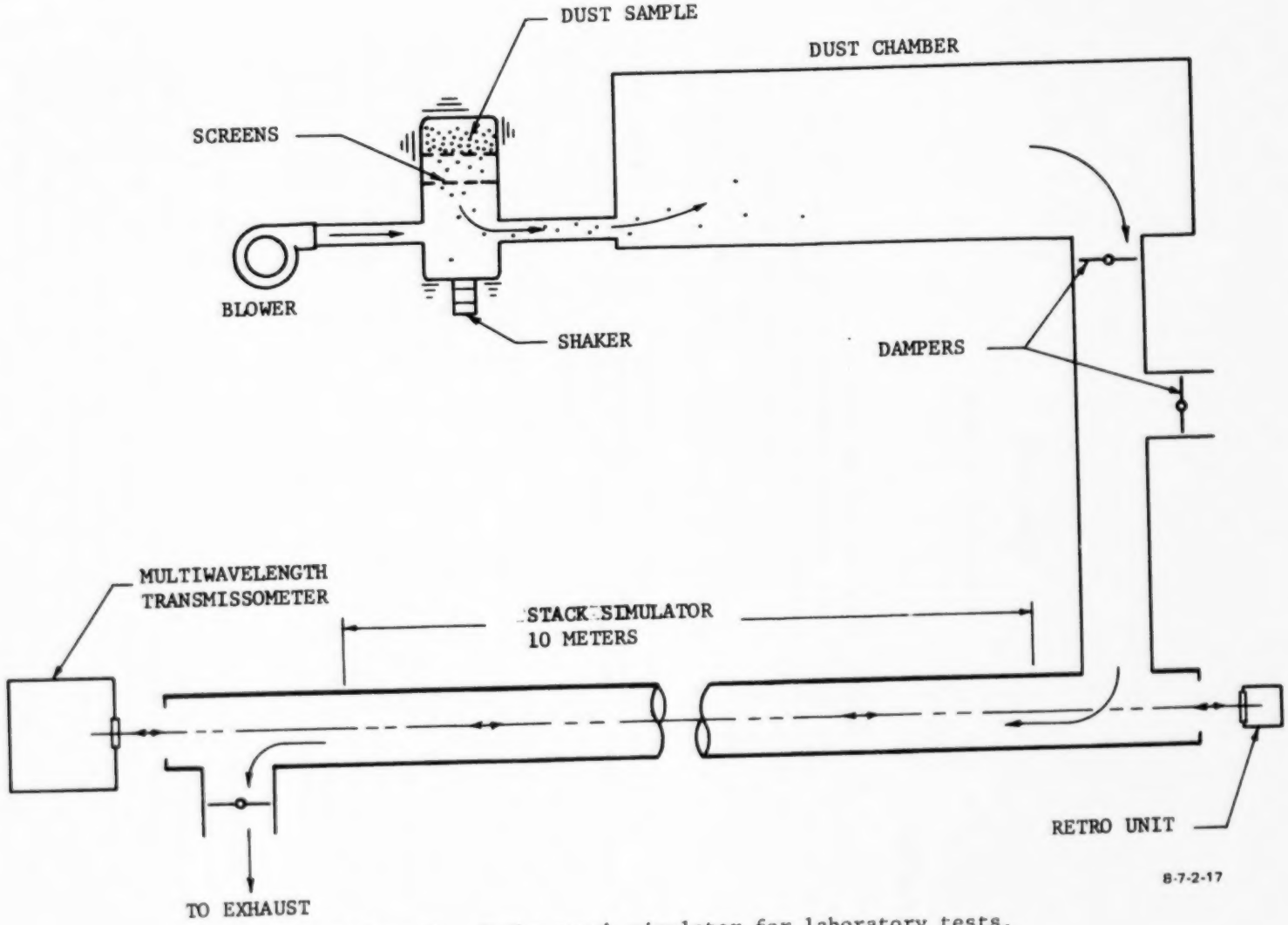

Figure 23. Smoke stack simulator for laboratory tests.

PARTICULATES

A multiwavelength transmissometer was used in earlier studies performed at a number of different industrial sites. The data obtained indicated that the particle size of the effluents in the stack was not constant with time but would change as plant operations changed (i.e., starting and stopping of the plant process, changing the feed materials, etc.), or when conditions in the pollution control system were altered (i.e., blowing or shaking bags, etc.). When samples were taken into the laboratory and redeployed using the dust chamber, the size distribution was generally constant and repeatable. This is not surprising since the observed distribution should be that of the feed sample appropriately corrected for the efficiencies and prejudices of the extraction system.

The material that was studied the most was the effluent from the kiln of a dry process cement plant. Initially, index measurements were made on both baghouse samples and chimney samples. When the optical properties proved to be the same, the more readily available baghouse samples were used. The material was taken from the freshly shaken bags while still hot (300^{o}C) and stored in sealed containers. As long as the sample was not exposed to laboratory air for undue lengths of time (i.e., overnight), it would flow freely through the feed sieves (67 micrometers to 125 micrometers). After exposure, the particulate would not shake through the sieves but could be brushed through. When sieved a second time, the results were the same. Apparently the material is hygroscopic and the particles develop a strong affinity for each other and would rather roll into balls than fall through the sieves.

In order to make measurements on cement dust samples of different sizes, it was decided to use fractionated cement dust as the raw feed material. Approximately 50 kg (110 lbs) of the virgin dust was shipped to a company that builds instruments that classify particles by size. When the samples were returned and did not flow through the feed sieves, it was obvious that they had been severely moisture contaminated. The unit that had been used in performing the classification suspended the particles in laboratory air which ran from 40 to 60 percent relative humidity.

A second attempt at classification was made with the unit completely enclosed in a polyethylene house into which flowed 3.4×10^{5} liters (12,000 cubic feet) of dry nitrogen. The sieving properties of most of the samples were improved, however, the small fractions (1 micrometer and less) would still not pass the sieves. Either the precautions taken were not sufficient or the ultrafine particles may have this inherent characteristic.

In order to obtain effluents with reduced mean radii, an alternative approach was adopted. The feed material used was the virgin dust but the flow characteristics of the chambers were altered to discriminate against large particles. The air flow in the stack simulator, normally 3 meters/second (10 feet/second), was reduced to 1.5 meters/second (5 feet/second). The feed damper from the dust chamber was replaced with a flow limiting screen while the fresh air damper was fully opened. This resulted in good log normal distributions with mean radii of 1.7 to 1.8 micrometers. In order to obtain a

larger mean radii, the air flow was set at 7.5 meters/second (25 feet/second) and the feed damper opened wide while the fresh air damper was replaced by a flow limiting screen. The sample used came from the classifier and had some of the fine material removed. This resulted in a slightly altered distribution with a mean radius of 3.0 to 3.1 micrometers.

ANALYSIS

The equations governing the key properties of a distribution of particles can be written

$$K(\lambda) = N_o \int_o^\infty p(r)dr\ \pi r^2\ Q(n,\lambda) \tag{3}$$

$$M_c = N_o \int_o^\infty p(r)dr\ 4/3\ \pi r^3\ \rho \tag{4}$$

Where $K(\lambda)$ is the wavelength dependence of the extinction, $p(r)\ dr$ is a dimensionless probability function (i.e., the probability that the size of a particle will fall between r and r + dr), N_o is the number of particles per unit volume, Q is the extinction efficiency, M_c the mass concentration, and ρ is the density of the material.

If the mass concentration is log normally distributed:

$$P(r) = \frac{1}{\sqrt{2\pi}\ \sigma} \int_o^r e^{\frac{-(\ln r - \ln ro)^2}{2\sigma^2}} \frac{dr}{r} \tag{5}$$

then $p(r)\ dr$ is given by:

$$p(r)\ dr = Ae^{\frac{-(\ln r - \ln r_o)^2}{2\sigma^2}} \frac{dr}{r^4} \tag{6}$$

where A is a normalizing constant such that:

$$\int_o^\infty p(r)dr = 1 \tag{7}$$

It can be shown that:

$$A = \frac{r_o^3\ e^{-9/2\ \sigma^2}}{\sqrt{2\pi}\ \sigma} \tag{8}$$

If it is necessary to truncate the integral of Equation (3) or (4) for computational purposes or for physical reasons (e.g., the particles have been subjected to the same size-limiting processes such as a cyclone), Equations (3) or (4) can be restated so as to be self-normalizing:

$$K(\lambda) = \frac{N_o \int_A^B p(r)\, dr\, \pi\, r^2\, Q(r,\lambda)}{\int_A^B p(r)dr} \tag{9}$$

$$M_C = \frac{N_o \int_A^B p(r)dr\ 4/3\ \pi r^3\ \rho}{\int_A^B p(r)\, dr} \tag{10}$$

While p(r) is a function of r, it is also a function of the distributional parameters and is more correctly

$$p(r,\ r_o,\ \sigma)$$

showing the dependence on the mean, r_o, and the spread, σ. If, for a given system of particles, the indices are known, then the Q functions are known. If p(r) is known to have a characteristic distributional form, then $K(\lambda)$ can be calculated once r_o, σ and N_o are known.

The value of $K(\lambda)$ can also be calculated from the measured transmission values

$$K(\lambda) = -\frac{\ln T(\lambda)}{L} \tag{11}$$

where L is the optical path length through the particulates and T is the transmission at a given wavelength.

The experimental data is processed in a way analagous to the curve fitting described in Section 4 (Figures 2, 3, and 4). For a given set of distributional parameters, the computer calculates the value of N_o needed to produce agreement between Equation (9) and Equation (11) at each wavelength. If the distribution selected was absolutely correct and the experimental data perfect, the calculated value of N_o would be independent of wavelength. Generally, this is not so and it is necessary to use a least squares procedure on N_o to evaluate the quality of the fit of Equation (9) to Equation (11). When the values of r_o and σ are found that give this best fit, they are used to calculate M_C using Equation (10). Since the computer time required to analyze the data is generally shorter than the time taken to acquire the data (for computer sampling rates of 1 set of observations per second), it is reasonable to predict that onboard minicomputers could be designed to produce near real-time monitoring systems.

TEST RESULTS

An extensive series of tests using cement particulates were undertaken to compare the mass concentration as measured with method 5 techniques to values calculated from the optical data. On occasion, the probe was fitted with an impactor so that the calculated size distribution could be directly compared with those sampled. Since the runs were typically 20 to 30 minutes long and the data acquisition system sampled the data about 10 times a second, approximately 15,000 sample sets were available for analysis. In order to conserve computer costs, every 10th set or every 60th set was analyzed, producing 250 to 1500 readouts per run. Each readout would include the best values of r_o for a given σ, the M_C associated with that r, and the residuals of the least squares fit. The average mass concentration for the entire run was also presented.

The value of r_o that occurred most frequently was 1.9 micrometers, with 2.0 micrometers a close second. In some runs the value stayed constantly at 1.9, in others it varied with time. Most variations occurred towards the end of a run and even then seldom fell outside of the range 1.9 to 2.2 micrometers. The values of σ generally ranged between 0.45 and 0.60. One run, number 21, appeared to have different properties. In this single instance r_o ranged between 2.4 and 2.7 micrometers and σ ranged between 0.85 and 0.95. Apparently the sample used for this run differed in some way from the others but still produced acceptable data.

The excellent agreement of the mass concentration data is shown in Figure 24. A perfect fit would require data points to fall along the indicated straight line. The data from a typical impactor run is shown in Figure 25. The data is best fit by a value of r_o of 1.9 micrometers and a σ of 0.60.

An experiment of more limited scope was attempted while trying to vary the particle size distribution in the manner described above. Because an electrical problem made it impossible to use the automatic data processing system, each run was limited to 10 or 15 data sets fed to the computer by hand. The results are summarized in Table 3.

Figures 26 and 27 show the log normal plots of the impactor runs while Figure 28 illustrates the agreement between experimentally determined and calculated values of the mass concentration.

In run number 8, virgin baghouse dust was used and the rate of extraction of particulate air reduced to enhance the relative abundance of small particles. The distribution still appears to be log normal over most of the range (i.e., 2 percent to 98 percent). The experimental data yields $r_o = 1.7$ micrometers and $\sigma = 0.45$, agreeing well with the optical data for runs 8 and 9. Runs 10 and 11 were performed in a manner similar to runs 8 and 9 except that the feed sieves were different. The optical data implies both a smaller mean and spread.

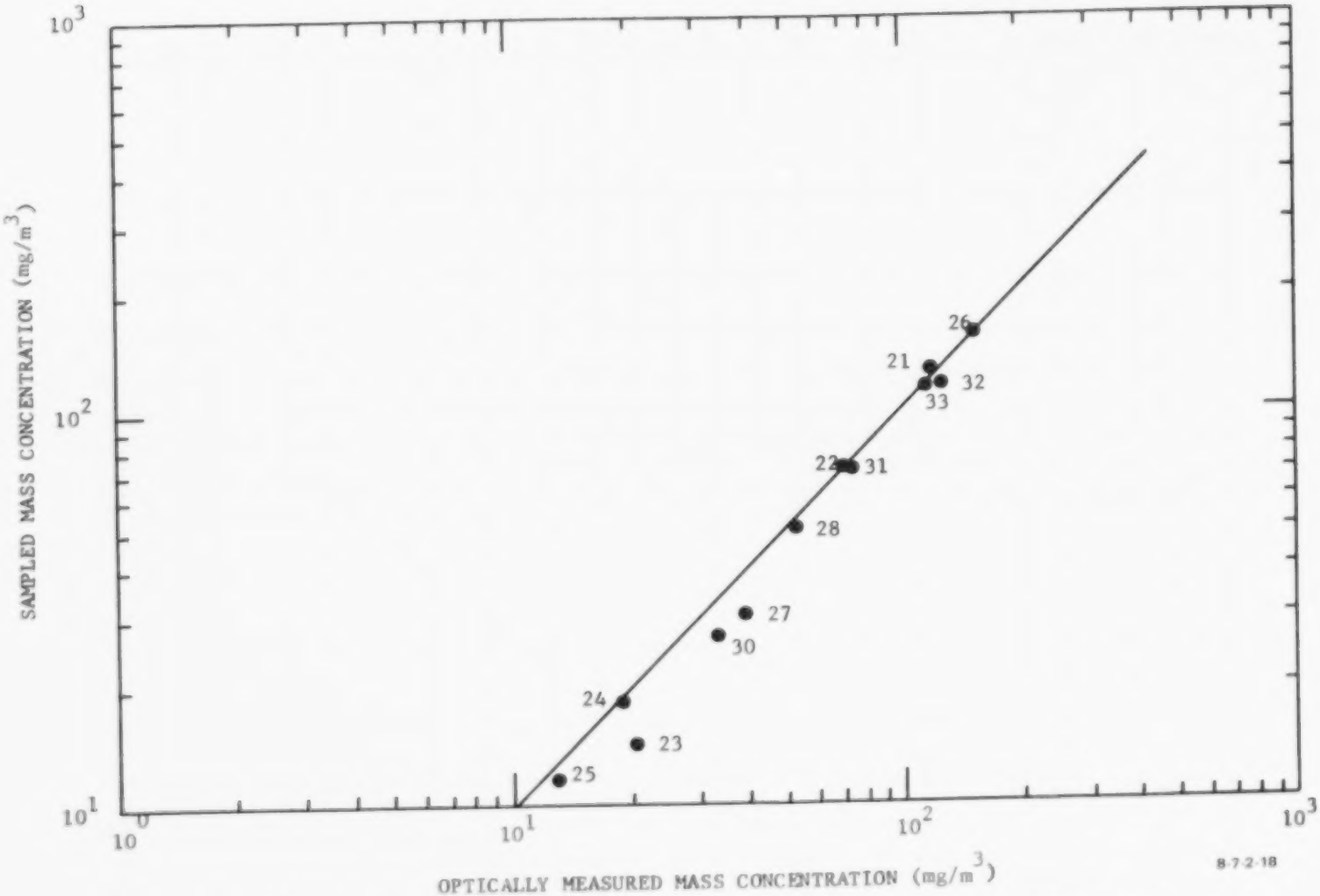

Figure 24. Mass concentration correlation between optical measurement and sampling measurement.

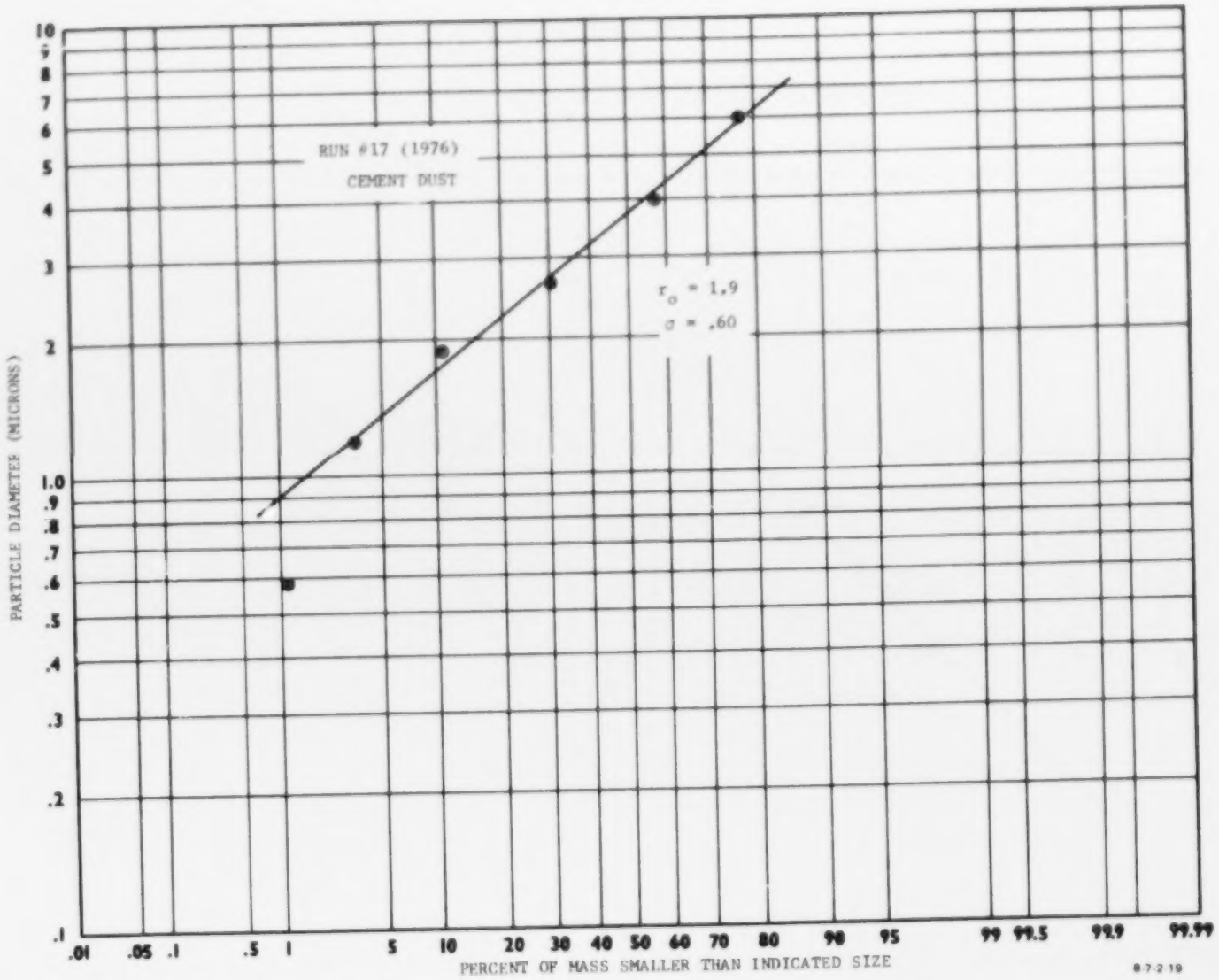

Figure 25. Particle size distribution function.

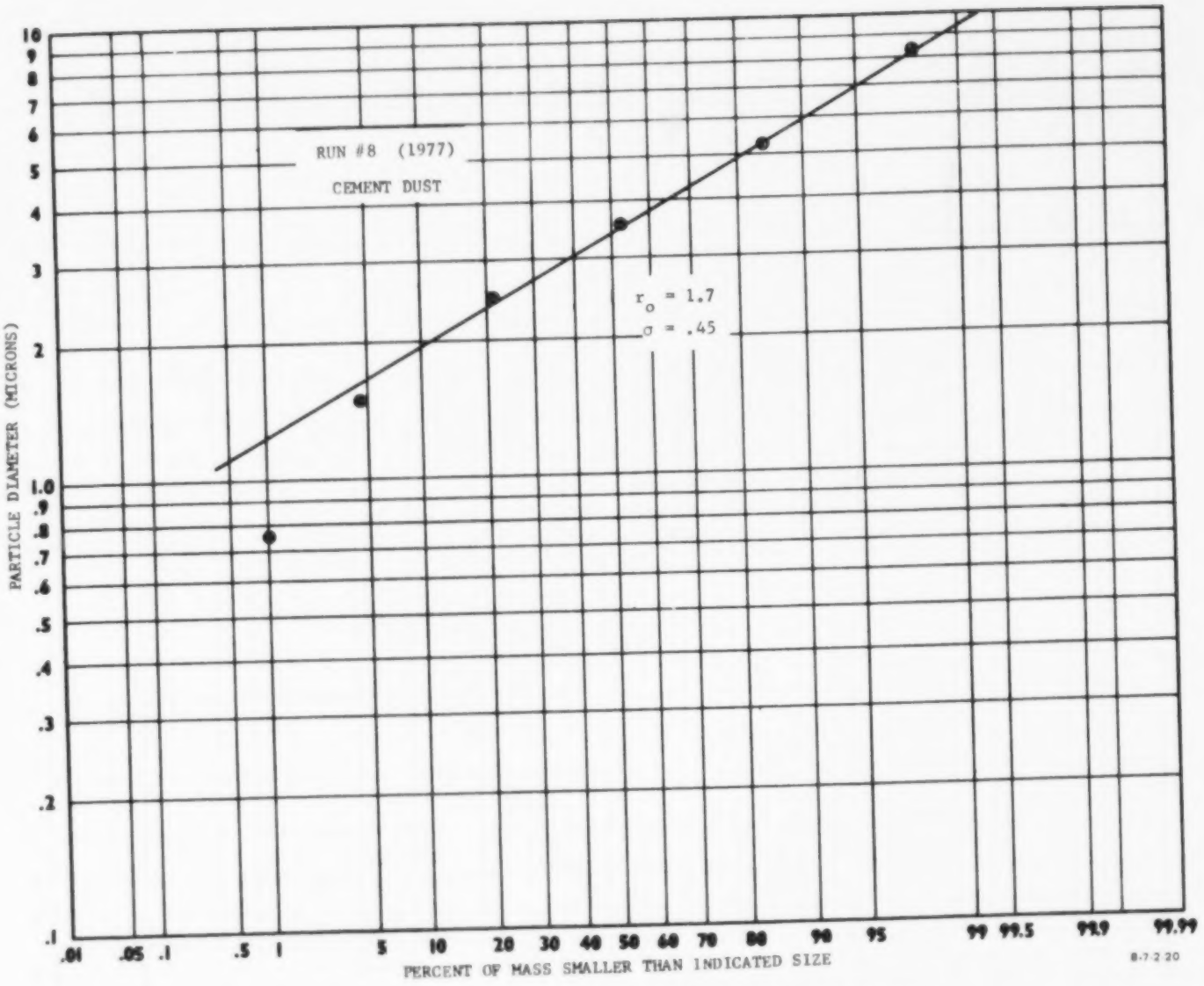

Figure 26. Particle size distribution function.

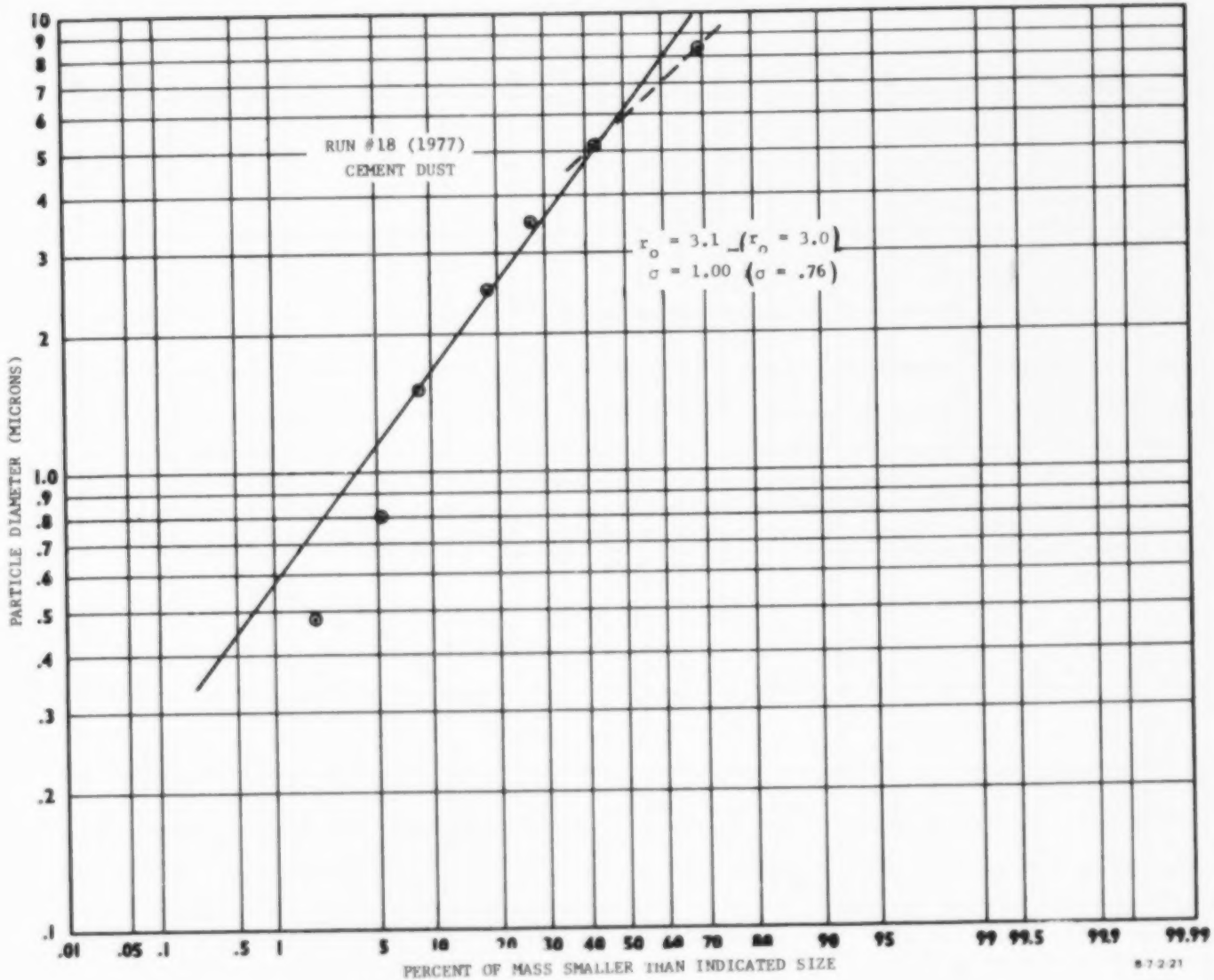

Figure 27. Particle size distribution function.

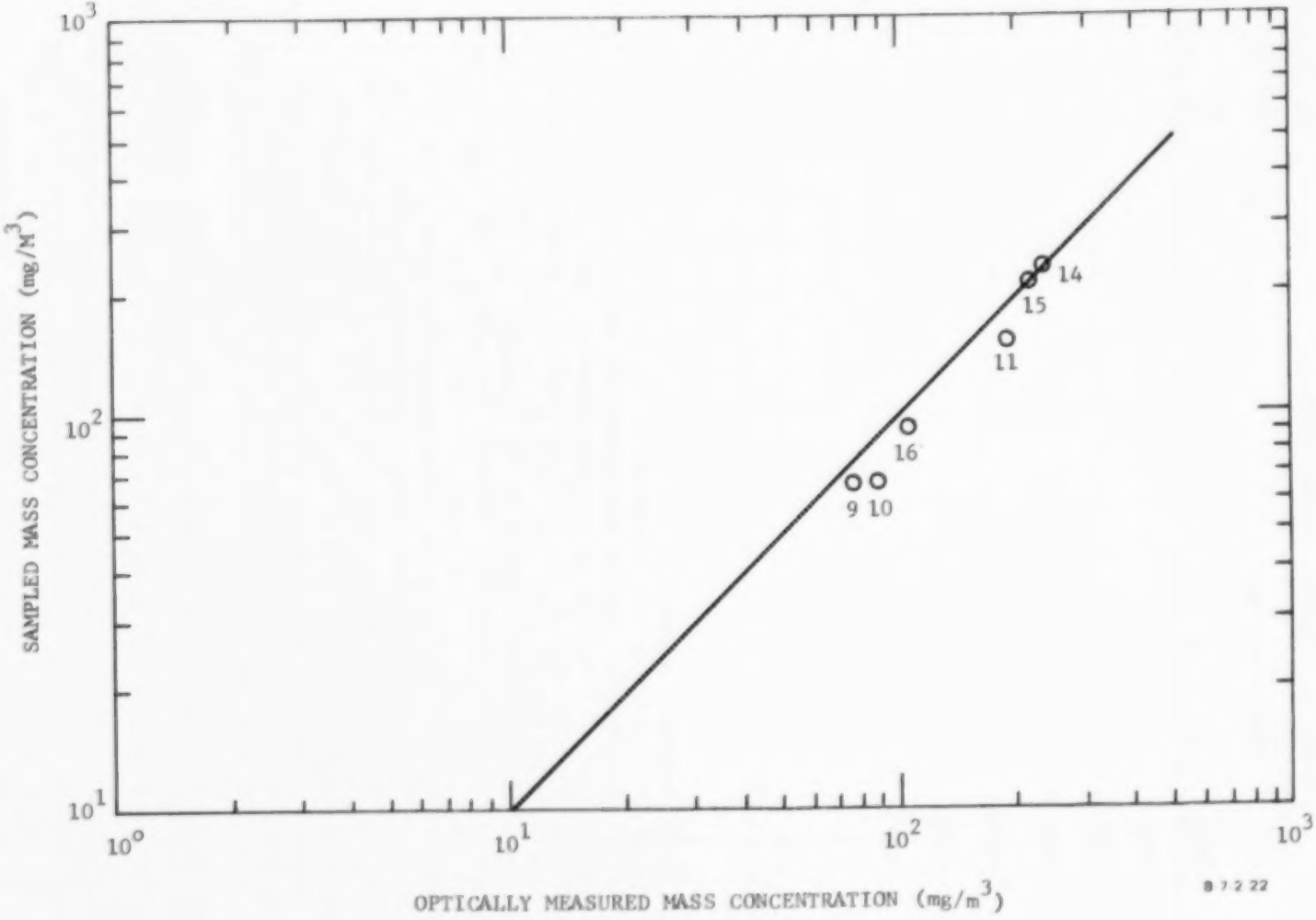

Figure 28. Mass concentration correlation between optical measurement and sampling measurement.

TABLE 3. SUMMARY OF TEST RESULTS

Experiment No.	Type	Monitored Data r_o	Monitored Data σ	Monitored Data M_C	Calculated Data r_o	Calculated Data σ	Calculated Data M_C
8	Imp.	1.7	0.45	-	1.7-1.8	4.5-.5	89.0
9	Method 5	-	-	67	1.7-1.8	0.4-0.45	77.0
10	Method 5	-	-	68	1.5	0.3	84.7
11	Method 5	-	-	157	1.5	0.3	189
14	Method 5	-	-	240	2.0-2.9	0.5-0.6	237
15	Method 5	-	-	220	2.4-2.9	0.5-0.6	216
16	Method 5	-	-	94	2.5-2.9	0.5-0.6	105
17	Imp	2.9	0.60	-	2.5-2.9	0.5-0.6	135

Runs 14 to 17 represent attempts to maximize r_o by using particles that were sent through the classifier and collected in the large particle output. This particular sample had been through the classifier three times and represented the residuals after a portion of the distribution below 9 micrometers had been removed. The dust chamber was also operated in a condition designed to enhance the number of larger particles. Had the original sample not been truncated by a cyclone operating upstream of the baghouse, the resulting distribution might have closely resembled a shifted log normal. The impactor run of Figure 27 shows a value of r_o = 3.1 μ and a σ of 1.00 based on the points in the 5 to 40 percentile. The 40 to 70 percentile points yield a value of r_o = 3.0 μ and σ = 0.76. The impactor was not designed to give data beyond this point (i.e., d = 8 micrometers). Were such points available, they would show a gross deviation from log normal, since the dust entering the baghouse has been passed through the cyclone and is relatively free of particles significantly larger than 10 μ. The computer interprets this truncation plus enrichment (affecting some 30 percent of the mass) as a reduced spread (i.e., σ = 0.55 to 0.60) and calculates r_o to range between 2.5 and 2.9 micrometers.

The fast extraction rates used to enhance the number of large particles make the observed results very dependent on feed rate. With slow extraction rates, irregularities in feed rates are averaged out. The results tend to be more constant and uniform with time. With fast extraction rates not only does the instantaneous value of the mass concentration fluctuate with feed irregularities but the size distribution also fluctuates. When the feed stops completely, the large particles disappear almost immediately while the fines can be seen (at reduced concentration) for several minutes. In experiment

No. 14, the feed supply began to run out before the end of the run and the value of r_o began to fall. In spite of the fluctuations, the calculated average values of the mass concentrations are always in close agreement with the measured values.

REFERENCES

1. Holland, A. C., and J. S. Draper. Analytical and Experimental Investigation of Light Scattering from Polydispersions of Mie Particles. Applied Optics, March, 1967. Vol. 6, No. 3.

2. Holland, A. C., and G. Gagne. The Scattering of Polarized Light by Polydisperse Systems of Irregular Particles. Applied Optics, May, 1970. Vol. 9, No. 5.

3. Querry, M. R., B. Curnutte, and D. Williams. Refractive Index of Water in the Infrared. Optical Society of America, October, 1969. Vol. 59, No. 10.

4. Irvine, W. M., and J. B. Pollack. Infrared Optical Properties of Water and Ice Spheres. ICARUS 8, 324-360 (1968).

5. Peterson, J. T., and J. A. Weinman. Physical Properties of Quartz Dust Particles at Infrared Wavelengths. Geophysical Research, December 20, 1969. Vol. 74, No. 28.

6. Twitty, J. T., and J. A. Weinman. Radiative Properties of Carbonaceous Aerosols. Journal of Applied Meterology, August, 1971, P 725.

7. Volz, F. E. Infrared Refractive Index of Atmospheric Aerosol Substances. Applied Optics, April, 1972. Vol. 11, No. 4.

8. Volz, F. E. Infrared Optical Constants of Ammonium Sulfate, Sahara Dust, Volcanic Pumice, and Flyash. Applied Optics, March, 1973. Vol. 12, No. 3.